



Aalborg Universitet

**AALBORG UNIVERSITY**  
DENMARK

## Use of a Series Voltage Compensator for Reduction of the DC-Link Capacitance in a Capacitor-Supported System

Wang, Huai; Chung, Henry Shu-Hung; Liu, Wenchao

*Published in:*

*I E E E Transactions on Power Electronics*

*DOI (link to publication from Publisher):*

[10.1109/TPEL.2013.2262057](https://doi.org/10.1109/TPEL.2013.2262057)

*Publication date:*

2014

*Document Version*

Accepted author manuscript, peer reviewed version

[Link to publication from Aalborg University](#)

*Citation for published version (APA):*

Wang, H., Chung, H. S-H., & Liu, W. (2014). Use of a Series Voltage Compensator for Reduction of the DC-Link Capacitance in a Capacitor-Supported System. *I E E E Transactions on Power Electronics*, 29(3), 1163-1175. <https://doi.org/10.1109/TPEL.2013.2262057>

### General rights

Copyright and moral rights for the publications made accessible in the public portal are retained by the authors and/or other copyright owners and it is a condition of accessing publications that users recognise and abide by the legal requirements associated with these rights.

- Users may download and print one copy of any publication from the public portal for the purpose of private study or research.
- You may not further distribute the material or use it for any profit-making activity or commercial gain
- You may freely distribute the URL identifying the publication in the public portal -

### Take down policy

If you believe that this document breaches copyright please contact us at [vbn@aub.aau.dk](mailto:vbn@aub.aau.dk) providing details, and we will remove access to the work immediately and investigate your claim.

© 2013 IEEE. Personal use of this material is permitted. Permission from IEEE must be obtained for all other uses, in any current or future media, including reprinting/republishing this material for advertising or promotional purposes, creating new collective works, for resale or redistribution to servers or lists, or reuse of any copyrighted component of this work in other works.

Digital Object Identifier (DOI): [10.1109/TPEL.2013.2262057](https://doi.org/10.1109/TPEL.2013.2262057)

IEEE Transactions on Power Electronics (in Press), online publication: 07 May 2013.

### **Use of a Series Voltage Compensator for Reduction of the DC-Link Capacitance in a Capacitor-Supported System**

Huai Wang  
Henry Shu-Hung Chung  
Wenchao Liu

#### **Suggested Citation**

H. Wang, H. S. H. Chung, and W. Liu, "A new concept of high-voltage DC–DC conversion using asymmetric voltage distribution on the switch pairs and hybrid ZVS–ZCS scheme," *IEEE Trans. on Power Electron.*, (in press). Online access: <http://dx.doi.org/10.1109/TPEL.2013.2262057>

**Title** : Use of a Series Voltage Compensator for Reduction of the DC-Link Capacitance in a Capacitor-Supported System

**Authors** : Huai WANG\*, *Member, IEEE*  
Henry Shu-hung CHUNG<sup>†</sup> (Corresponding author), *Senior Member, IEEE*  
Wenchao LIU<sup>†</sup>

**Address** : \* Center of Reliable Power Electronics (CORPE)  
Department of Energy Technology  
Aalborg University  
Pontoppidanstraede 101, DK-9220 Aalborg  
Denmark

<sup>†</sup> Centre for Smart Energy Conversion and Utilization Research (CSCR)  
City University of Hong Kong  
Tat Chee Avenue, Kowloon Tong  
Kowloon, Hong Kong

**Tel.** : (852) 3442 7807

**Email** : eeshc@cityu.edu.hk

# Use of a Series Voltage Compensator for Reduction of the DC-Link Capacitance in a Capacitor-Supported System

Huai WANG\*, Henry Shu-hung CHUNG<sup>†</sup> and Wenchao LIU<sup>†</sup>

*Abstract* - A technique for reduction of the dc-link capacitance in a capacitor-supported system is presented. The concept is based on connecting a voltage source in series with the dc bus line to compensate the ripple voltage on the dc-link capacitor, so as to make the output have a near zero ripple voltage. Since the voltage compensator processes small ripple voltage on the dc link and reactive power only, it can be implemented with low-voltage devices. The overall required energy storage of the dc-link, formed by a reduced value of dc-link capacitor and the voltage compensator, is reduced, allowing the replacement of popularly used electrolytic capacitors with alternatives of longer lifetime, like power film capacitors, or extending the system lifetime even if there is a significant reduction in the capacitance of electrolytic capacitors due to the aging effect. Comprehensive analysis on the static and dynamic characteristics of the system, and hold-up time requirement will be discussed. The proposed technique is exemplified on an ac-dc-dc power conversion system. Theoretical predictions are favorably verified by experimental results.

*Keywords*- dc-link capacitor, power conversion system, capacitance reduction, voltage compensator

## NOMENCLATURE

$C$	Dc-link capacitor
$C_{DC}$	Input capacitor of the voltage compensator
$L_f$	Output filter inductance of the voltage compensator
$C_f$	Output filter capacitance of the voltage compensator
$v_{ab}$	Output voltage of the voltage compensator
$V_{ab}$	Amplitude of $v_{ab}$
$V_{ab,rms}$	Root-mean-square value of $v_{ab}$
$v_C$	Dc-link voltage
$V_C$	Dc component of $v_C$
$v_C(0)$	Voltage of $v_C$ in the event of an input power outage of the front-end converter [ $v_C(0) = V_C -  \Delta v_C $ ]
$\Delta v_C$	Ac component of $v_C$
$\Delta V_{C,rms}$	Root-mean-square value of $\Delta v_C$
$ \Delta v_C $	Amplitude of $\Delta v_C$
$v_{con}$	Control signal in the control stage of the voltage compensator
$V_{con}$	Amplitude of $v_{con}$
$v_d$	Output voltage of the dc-link module
$V_{d,min}$	Specified minimum dc-link voltage during the hold-up time period
$V_D$	Dc component of $v_d$
$ \Delta v_d $	Amplitude of the voltage ripple component of $v_d$
$v_{DC}$	Input voltage of the voltage compensator

$V_{DC,ref}$	Input voltage reference of the voltage compensator
$v_{DC,min}$	Minimum value of $v_{DC}$
$v_{DC}(0)$	Voltage of $v_{DC}$ in the event of an input power outage of the front-end converter [ $v_{DC}(0) = v_{DC,ref}$ ]
$ \Delta v_{DC} $	Amplitude of the voltage ripple component of $v_{DC}$
$v_{os}$	Offset voltage in the control stage of the voltage compensator
$V_{os}$	Dc component of $v_{os}$
$ \Delta v_{os} $	Amplitude of the voltage ripple component of $v_{os}$
$v_{out}$	Output voltage of the phase-shifted full-bridge dc-dc converter
$v_{tri}$	Carrier signal of the PWM of the voltage compensator
$V_{tri}$	Amplitude of $v_{tri}$
$i_a$	Current flowing through the input side of the dc-link capacitor/module bus line
$I_A$	Dc component of $i_a$
$\Delta i_a$	Ac component of $i_a$
$ \Delta I_a $	Amplitude of $\Delta i_a$
$i_C$	Current following through the dc-link capacitor $C$
$ \Delta I_C $	Amplitude of $i_C$
$i_{cf}$	Current flowing through $C_f$
$i_d$	Current flowing through the output side of the dc-link capacitor/module bus line
$I_{d,rms}$	Root-mean-square value of $i_d$
$I_D$	Dc component of $i_d$

$\Delta i_d$	Ac component of $i_d$
$ \Delta I_d $	Amplitude of $\Delta i_d$
$i_{out}$	Output current of the phase-shifted full-bridge dc-dc converter
$f_{rip}$	Frequency of $\Delta v_C$
$M$	Modulation index of ratio $V_{con} / V_{tri}$
$P_{ab}$	Average power absorbed by the voltage compensator
$S_{ab}$	Apparent power handled by the voltage compensator
$S_m$	Apparent power handled by the main circuit
$T$	Least common multiple of $2\pi / \omega_1$ and $2\pi / \omega_2$
$\alpha$	Scaling factor of $v_C$ in the control stage to the PWM controller
$\beta$	Ratio between $ \Delta I_C $ and $I_D$
$\gamma$	Ratio between $v_{DC}(0)$ and $ \Delta v_C $
$\delta_1$	Phase of $\Delta i_a$
$\delta_2$	Phase of $\Delta i_d$
$\lambda$	Ratio between $C$ and $C_{DC}$
$\mu$	Ratio between $ \Delta v_C $ and $V_C$
$\rho$	Ratio between $V_{d,min}$ and $V_C$
$\omega$	Angular frequency of the capacitor ripple current ( $\omega = 2\pi f_{rip}$ )
$\omega_1$	Frequency of $\Delta i_a$
$\omega_2$	Frequency of $\Delta i_d$
$N$	Number of hold-up cycles with respect to the period of the dc-link voltage ripple with the proposed dc-link module

## I. Introduction

A capacitor-supported system consists of multiple power converters interconnected by a dc link. The dc-link voltage is maintained by a capacitor bank that absorbs instantaneous power difference between the input source and output load, minimizing voltage variation on the dc link, and providing sufficient energy during the hold-up time of the system. Among different types of capacitor, aluminum electrolytic capacitors (E-Caps) are the most popular choice because of their high volumetric efficiency and low cost. However, they suffer from the drawbacks of high equivalent series resistance (ESR); low ripple current capability; bottleneck of the voltage rating; relatively short lifetime compared to other components and considerable maintenance work.

Advances in power film capacitor technology are emerging for dc-link filtering [1]-[2]. Power film capacitors outperform aluminum E-Caps in terms of ESR, self-healing capability, life expectancy, environmental performance, dc-blocking capability, ripple current capability and reliability. Although low-voltage and high-value film capacitors are available, the capacitance of the high-voltage film capacitors still cannot compete with E-Caps, due to their relatively low volumetric efficiency and high cost. To lessen the dependency of the dc-link capacitance, there are many prior-art methods, based on the following approaches:

- 1) *Performance trade-off* - This method allows a larger voltage ripple across the dc-link with a smaller capacitance. However, it is practically less impressive as the system performance will be degraded. It is more suitable for certain applications, like the ones in [3]-[5]. A set of design procedure is given in [6] for the optimization of capacitor bank.
- 2) *Reduction of the dc-link capacitor current with sophisticated control*. The concept is based on reducing the ripple current flowing through the dc-link capacitor [7]-[12]. The front-stage converter is an active rectifier in [7]-[10], and a step-up dc-dc converter in



[11]-[12], while the output is an inverter. Their key advantage is that no additional circuit is needed. However, those control methods cannot be applied to systems with front-end diode-bridge rectifier. Apart from requiring a sophisticated controller, some of them also rely on specific relationship in the operating frequency between the converters connected [7], [10], and [11]. The method given in [8] is limited to three-phase systems. The controller described in [7] is based on assuming an ideal energy conversion. Thus, the actual input current would be distorted unless multiple cell load inverters are used. The performance of those controllers is greatly dependent on the accuracy of the computations [9], [12] and affected by the overall time delays of the control loops.

- 3) *Increase in the frequency of the dc-link voltage ripple.* A double frequency front-end converter with multi-phase switching is proposed in [13] to reduce the ripple voltage. However, the approach cannot reduce the dc-link capacitance significantly.
- 4) *Ripple cancellation circuit with a coupled element.* In [14], a coupled inductor is applied to cancel the voltage ripple of the dc input, dc output or dc-link of a power converter. The concept is based on assuming that the capacitor used in the storage tank is infinite. But, in reality, the capacitance has a finite value, and the coupled inductor filter and the capacitor form a low pass filter. To avoid large-sized coupled windings, the technique is more suitable for filtering high-frequency ripples or noise, such as switching ripple, EMI filtering. Moreover, the dynamic response of the capacitor may be degraded due to the series-connected coupled winding.

Apart from the aforementioned methods, active power filters can also be used for reduction of the dc-link capacitance as presented in [15]-[28]. It is based on connecting an auxiliary circuit in parallel with the dc-link capacitor. The added circuit serves as an active

impedance or energy source. Different methods of implementing the auxiliary circuit are given. In [16], the auxiliary circuit has a single switch with a dissipative resistor. In [20], a relay is placed at the input line and is activated, depending on the dc-link voltage level, resulting in a stable dc-link voltage, but at the expense of reducing the input power factor of the entire system. In [15], [17] and [22], an H-bridge circuit with a current source (inductor) is used to minimize the ripple current of the dc-link capacitor. However, the high inductor current stress and high switching frequency requirement in [22] are the major practical challenges of the method. A current injection method was applied in [18]-[19], [21] and [23] by a half-bridge structure. In [24]-[25], a two-switch converter that can operate bi-directionally in both buck and boost modes is used for the H-bridge front-end and dc current electrical load application. In [26], a series-connected dual boost converter is as the shunt active filter for a three-phase diode rectifier front-end conversion system. In [27], the ripple reduction circuit allows an additional power port for enhancing the dynamic response of the whole system. In [28], a single switch, diode and capacitor circuit is added in parallel with the input capacitor of a microinverter to reduce the overall capacitance requirement. The common challenge of all these methods is that the components used in the auxiliary circuit are under a high voltage stress, which could be as high as the dc-link voltage. Moreover, the impact of the active filters on the hold-up behavior of the dc-link has not been explored in [15]-[28].

This paper presents a module that can reduce the required dc-link capacitance. Its operating principle is based on connecting a series voltage source between the dc-link capacitor and the load. The energy storage in the whole system is reduced, making it possible to replace the high-value E-Caps with low-value high-performance capacitors. The voltage compensator is of low voltage and low power rating, as it only produces low voltage and handles reactive power.

## II. Proposed Module for DC-Link Capacitance Reduction

Fig. 1 illustrates the basic concept of the module for reducing the dc-link capacitance. The module is composed of a capacitor  $C$  and a voltage source  $v_{ab}$ . The module is connected between two converters, namely Converter 1 and Converter 2. The capacitor voltage  $v_C$  has dc component  $V_C$  and ripple voltage  $\Delta v_C$ . The peak-to-peak value and ripple frequency of  $\Delta v_C$  are  $2|\Delta v_C|$  and,  $f_{rip}$  respectively.  $v_{ab}$  is connected in series between the capacitor  $C$ ,  $v_C$ , and the input of Converter 2,  $v_d$ . It generates a voltage counteracting  $\Delta v_C$  with its dc component equal to zero (i.e.,  $v_{ab} = \Delta v_C$ ). Thus,  $v_d$  has the same dc value as that across  $C$ , but with a zero ripple voltage in the ideal condition. Such architecture allows a high voltage ripple on  $C$ , implying that the value of  $C$  can be made smaller, but at the expense of increasing the magnitude of  $v_{ab}$ .

$v_{ab}$  is a dc-ac converter with a full-bridge (FB) circuit and an output filter formed by the inductor  $L_f$  and the capacitor  $C_f$ . A half-bridge circuit can also be used if the current  $i_d$  is unidirectional. The dc side of the FB is connected to a dc voltage source, like a capacitor or a voltage source, with voltage  $v_{DC}$ . The gate signals for the switches  $S_1 \sim S_4$  in the FB are generated by a PWM modulator. Depending on the type of the dc source used, the control signal  $v_{con}$  is obtained by sensing different parameters. There are two possible configurations. The first one utilizes a capacitor for the dc source while the second one has an external supply connected to it. Since the first configuration gives a simpler solution, it will be studied in this paper.

Fig. 2 shows the control mechanism. The dc-link voltage  $v_C$  and the input voltage of the voltage compensator  $v_{DC}$  are sensed. The scaling factor  $\alpha$ , as will be shown later, is equal to the ratio between  $V_{tri}$  and  $V_{DC,ref}$ . The difference between  $V_{DC,ref}$  and  $v_{DC}$  is averaged by a low-pass

filter  $F(s)$  and processed by a PI controller  $G(s)$  to give an offset voltage  $v_{os}$ . The control signal  $v_{con}$  is derived by combining  $\alpha v_C$  with  $v_{os}$ . The dc component of  $\alpha v_C$  is ideally cancelled in  $v_{con}$  by  $v_{os}$  as  $V_{os} = -\alpha V_C$ , where  $V_{os}$  and  $V_C$  are the dc component of  $v_{os}$  and  $v_C$ , respectively. With such arrangement, it is unnecessary to use a high-pass filter to extract the ac component of  $v_C$ . At the same, the dc component of  $v_{ab}$  can be eliminated so that the added voltage source only handles ac component. During steady-state operation,  $v_{con}$  equals the conditioned ac component of  $\alpha v_C$ . It is then used to compare with the triangular carrier waveform in the PWM modulator to generate the voltage  $v_{ab}$  having the same phase and amplitude of  $\Delta v_C$ . Without any external supply, the power consumed by the module (i.e. power losses) is obtained from the ac side of the bridge, that is, Converter 1. Practically, instead of a pure ac voltage,  $v_{ab}$  and thus  $v_{con}$  have a small dc component.

A dc analysis of the circuit shown in Fig. 1 gives

$$V_D = V_C \quad (1)$$

$$I_D = I_A \quad (2)$$

$\Delta i_a$  and  $\Delta i_d$  are expressed as

$$\Delta i_a(t) = |\Delta I_a| \sin(\omega_1 t + \delta_1) \quad (3)$$

$$\Delta i_d(t) = |\Delta I_d| \sin(\omega_2 t + \delta_2) \quad (4)$$

$\Delta i_a$  and  $\Delta i_d$  can be of any periodic form with multiple frequency components. Without loss of generality, only sinusoidal components of frequencies  $\omega_1$  and  $\omega_2$  are considered for  $\Delta i_a$  and  $\Delta i_d$ , respectively.  $\Delta v_C$  and  $v_{ab}$  can be expressed as

$$\begin{aligned}
v_{ab}(t) = \Delta v_C(t) &= \frac{1}{C} \int [i_a(t) - i_d(t)] dt \\
&= \frac{|\Delta I_a|}{\omega_1 C} \sin(\omega_1 t + \delta_1 - 90^\circ) - \frac{|\Delta I_d|}{\omega_2 C} \sin(\omega_2 t + \delta_2 - 90^\circ)
\end{aligned} \tag{5}$$

Based on (4) and (5),  $P_{ab}$  in a period  $T$  is given by

$$\begin{aligned}
P_{ab} &= \frac{1}{T} \int_0^T v_{ab}(t) i_d(t) dt \\
&= \frac{|\Delta I_d| |\Delta I_a|}{2 \omega_1 C T} \int_0^T \sin[(\omega_1 - \omega_2)t + (\delta_1 - \delta_2)] dt
\end{aligned} \tag{6}$$

The proof of (6) is given in appendix. It can be noted that  $P_{ab}$  equals zero except in a special case when  $\omega_1 = \omega_2$  and  $\delta_1 \neq \delta_2$ . Therefore, the voltage compensator ideally handles reactive power only in all of the other cases. For the special case concerned, the dc-link capacitance can be reduced by the synchronization control of the phases  $\delta_1$  and  $\delta_2$  [10].

The apparent power  $S_{ab}$  handled by the voltage compensator is

$$\begin{aligned}
S_{ab} &= V_{ab,rms} I_{d,rms} = \Delta V_{C,rms} I_{d,rms} \\
&= \frac{1}{2 \omega_1 C} \sqrt{[|\Delta I_a|^2 + (\frac{\omega_1}{\omega_2})^2 |\Delta I_d|^2](2I_D^2 + |\Delta I_d|^2)}
\end{aligned} \tag{7}$$

where  $\Delta V_{C,rms}$  is the root-mean-square (RMS) value of  $\Delta v_C$ .

Comparing with the apparent power of the main power conversion system

$S_m = V_D I_{d,rms} = V_C I_{d,rms}$ , the ratio between  $S_{ab}$  and  $S_m$  is

$$\frac{S_{ab}}{S_m} = \frac{\Delta V_{C,rms}}{V_C} \tag{8}$$

As  $\Delta V_{C,rms} \ll V_C$ , the apparent power rating of the voltage compensator (i.e.,  $S_{ab}$ ) is much smaller than that of the main system.

The relationship between the steady-state value of  $V_{ab}$  and  $V_{DC,ref}$  is expressed as

$$\begin{aligned}
 V_{ab} &= \frac{V_{con}}{V_{tri}} V_{DC,ref} \\
 &= \frac{\alpha |\Delta v_C| + |\Delta v_{os}|}{V_{tri}} V_{DC,ref} \\
 &= M V_{DC,ref}
 \end{aligned} \tag{9}$$

where  $M = \frac{V_{con}}{V_{tri}} = \frac{\alpha |\Delta v_C| + |\Delta v_{os}|}{V_{tri}}$  and  $|\Delta v_{os}|$  is the amplitude of the ripple voltage of  $v_{os}$ .

Ideally,  $v_{os}$  is a dc voltage. Thus,  $|\Delta v_{os}| = 0$ . As  $V_{ab} = |\Delta v_C|$ ,

$$\alpha = \frac{V_{tri}}{V_{DC,ref}} \tag{10}$$

Consider the control mechanism in Fig. 2,

$$\begin{aligned}
 v_{ab}(t) &= \frac{\alpha v_C(t) + v_{os}(t)}{V_{tri}} v_{DC}(t) \\
 &= [m_{a1} \sin(\omega_1 t + \delta_1 - 90^\circ) - m_{a2} \sin(\omega_2 t + \delta_2 - 90^\circ) + \frac{\alpha V_C + v_{os}(t)}{V_{tri}}] v_{DC}(t)
 \end{aligned} \tag{11}$$

where  $m_{a1} = \frac{\alpha |\Delta I_a|}{\omega_1 C V_{tri}}$  and  $m_{a2} = \frac{\alpha |\Delta I_d|}{\omega_2 C V_{tri}}$ .

Fig. 3 shows the waveforms of the dc-link capacitor voltage  $v_C$ , modulating signal  $v_m$ , carrier signal  $v_{tri}$ , and the voltage across  $C_{DC}$ ,  $v_{DC}$ . To study the voltage ripple across  $C_{DC}$ ,  $t_0$  and  $t_1$  in Fig. 3 are defined as the two time instants when  $\Delta v_C$  is across zero within one period. During the time interval from  $t_0$  to  $t_1$ ,  $C_{DC}$  is being charged by the load current and its voltage increases from minimum to maximum. The introduction of the third term  $[\alpha V_C + v_{os}(t)] / V_{tri}$  in (11) is related to the dc component of  $v_{ab}$  due to asymmetrical switching or power losses in the voltage compensator in practical operation, which has negligible impact on the steady-state

voltage ripple across  $C_{DC}$ . Therefore, it is neglected in the following analysis of the voltage ripple across  $C_{DC}$ . Based on Fig. 3 and the SPWM principle discussed in [29], the voltage across  $C_{DC}$  between  $t_0$  and  $t_1$  is given by

$$\begin{aligned}
v_{DC}(t) &= v_{DC,\min} + \frac{1}{C_{DC}} \int_{t_0}^{t_1} [I_D + |\Delta I_d| \sin(\omega_2 t + \delta_2) - i_{cf}(t)] \\
&\quad \times [m_{a1} \sin(\omega_1 t + \delta_1 - 90^\circ) - m_{a2} \sin(\omega_2 t + \delta_2 - 90^\circ)] dt \\
&= v_{DC,\min} + \frac{1}{C_{DC}} \left\{ \begin{aligned} &I_D \int_{t_0}^{t_1} [m_{a1} \sin(\omega_1 t + \delta_1 - 90^\circ) - m_{a2} \sin(\omega_2 t + \delta_2 - 90^\circ)] dt \\ &+ m_{a1} |\Delta I_d| \int_{t_0}^t \sin(\omega_1 t + \delta_1 - 90^\circ) \sin(\omega_2 t + \delta_2) dt \\ &+ m_{a2} |\Delta I_d| \int_{t_0}^t \sin(\omega_2 t + \delta_2) \cos(\omega_2 t + \delta_2) dt \\ &- \int_{t_0}^{t_1} i_{cf}(t) [m_{a1} \sin(\omega_1 t + \delta_1 - 90^\circ) - m_{a2} \sin(\omega_2 t + \delta_2 - 90^\circ)] dt \end{aligned} \right\} \quad (12)
\end{aligned}$$

From  $t_0$  to  $t_1$ , the net charge of the filter capacitor  $C_f$  by  $i_{cf}$  is zero, therefore, when  $\omega_1 \neq \omega_2$ , the voltage ripple on  $C_{DC}$ ,  $2|\Delta v_{DC}|$ , is given by

$$\begin{aligned}
2|\Delta v_{DC}| &= \frac{1}{C_{DC}} \{ I_D \int_{t_0}^{t_1} [m_{a1} \sin(\omega_1 t + \delta_1 - 90^\circ) - m_{a2} \sin(\omega_2 t + \delta_2 - 90^\circ)] dt \} \\
&= -\frac{m_{a1} I_D}{\omega_1 C_{DC}} [\sin(\omega_1 t_1 + \delta_1) - \sin(\omega_1 t_0 + \delta_1)] + \frac{m_{a2} I_D}{\omega_2 C_{DC}} [\sin(\omega_2 t_1 + \delta_2) - \sin(\omega_2 t_0 + \delta_2)] \quad (13)
\end{aligned}$$

For practical applications when  $\omega_1 \ll \omega_2$ , the effect of the second terms of (5) and (13) are negligible, and  $\sin(\omega_1 t_1 + \delta_1) = -1$ ,  $\sin(\omega_1 t_0 + \delta_1) = 1$ . Therefore,

$$2|\Delta v_{DC}| = \frac{2 m_{a1} I_D}{\omega_1 C_{DC}} \quad (14)$$

The above equation is also applicable for the case when  $\omega_2$  is even multiples of  $\omega_1$  as  $\sin(\omega_2 t_1 + \delta_2) = \sin(\omega_2 t_0 + \delta_2)$ . The voltage across  $C_{DC}$  is therefore presented by

$$v_{DC}(t) = V_{DC} + \frac{m_{a1} I_D}{\omega_1 C_{DC}} \sin(\omega_1 t + \delta_1) \quad (15)$$

The output voltage of the voltage compensator  $v_{ab}$  is

$$\begin{aligned} v_{ab}(t) &= [V_{DC} + \frac{m_{a1} I_D}{\omega_1 C_{DC}} \sin(\omega_1 t + \delta_1)] [m_{a1} \sin(\omega_1 t + \delta_1 - 90^\circ) - m_{a2} \sin(\omega_2 t + \delta_2 - 90^\circ)] \\ &\approx V_{DC} [m_{a1} \sin(\omega_1 t + \delta_1 - 90^\circ) - m_{a2} \sin(\omega_2 t + \delta_2 - 90^\circ)] - \frac{m_{a1}^2 I_D}{2 \omega_1 C_{DC}} \sin(2\omega_1 t + 2\delta_1) \end{aligned} \quad (16)$$

The first term of (16) is used to cancel the dc-link voltage ripple while the second term is a double frequency ripple, generating voltage variation on  $v_d$ . Thus, the voltage ripple of  $v_d$  is

$$2 |\Delta v_d| = \frac{m_{a1}^2 I_D}{\omega_1 C_{DC}} \quad (17)$$

### III. Hold-up Time Analysis of the DC-Link Module

The hold-up time of the system with and without the proposed module are compared in the following. After a loss of the input power, the energy stored in the dc-link module (i.e., the dc-link capacitor and the capacitor connected to the dc source) will be solely delivered to the load. In the following analysis, the hold-up time  $t_h$  is defined as the time duration between the start of the supply outage (i.e.,  $i_a = 0$ ) and the voltage  $v_d$  reduces to the minimum dc bus voltage  $V_{d,\min}$ . Fig. 4 (a) shows the timing diagram of two consecutive hold-up intervals distinguished by value of the modulation index  $M$  of the PWM modulator in Fig. 1. Figs. 4(b) and 4(c) show the equivalent circuits of the two intervals  $[0, t_{h1}]$  and  $[t_{h1}, t_{h2}]$ , respectively. For the sake of simplicity in the analysis, the power loss of the voltage compensator is neglected and the dc-link module is connected to a constant power load  $P_L$ .



1. *Initial state ( $t = 0$ ):*

Consider the worst case scenario. The voltage across the dc-link capacitor at the supply outage time (i.e.,  $t = 0$ ) is  $v_C(0) = V_C - |\Delta v_C|$ . The voltage across  $C_{DC}$ ,  $v_{DC}(0)$ , equals  $V_{DC,ref}$ . The voltage ripple across the dc-link capacitor is fully compensated by  $v_{ab}$ , implying

$$v_{ab}(0) = |\Delta v_C| = M v_{DC}(0) \quad (18)$$

where  $M = \frac{\alpha |\Delta v_C(0)|}{V_{tri}}$ .

2. *Stage I  $[0, t_{h1}]$  -  $M \leq 1$*

$t_{h1}$  is the time instant at which  $M = 1$ . Thus,

$$\frac{\alpha \Delta v_C(t_{h1})}{V_{tri}} = 1 \quad (19)$$

$$v_{ab}(t_{h1}) = \Delta v_C(t_{h1}) = -v_{DC}(t_{h1}) \quad (20)$$

Based on (18)-(20),

$$\Delta v_C(t_{h1}) = v_{DC}(0) \quad (21)$$

$$\begin{aligned} v_d(t_{h1}) &= V_C - \Delta v_C(t_{h1}) - v_{ab}(t_{h1}) \\ &= V_C - v_{DC}(0) + v_{DC}(t_{h1}) \end{aligned} \quad (22)$$

In this stage, the variation of  $v_d$  is small. Thus, the current  $i_d$  is assumed to be constant and is equal to  $I_D$ . Thus,

$$\Delta v_C(t_{h1}) = |\Delta v_C| + \frac{I_D}{C} t_{h1} = v_{DC}(0) \quad (23)$$

and

$$t_{h1} = \frac{C}{I_D} [v_{DC}(0) - |\Delta v_C|] = \frac{\beta}{\omega} (\gamma - 1) \quad (24)$$

By applying the conservation of energy between the energy delivery from the whole dc-

link module and the load consumption,

$$\frac{1}{2} C v_C^2(0) + \frac{1}{2} C_{DC} v_{DC}^2(0) - \frac{1}{2} C v_C^2(t_{h1}) - \frac{1}{2} C_{DC} v_{DC}^2(t_{h1}) = P_L t_{h1} \quad (25)$$

Based on (25),

$$v_{DC}(t_{h1}) = \mu \sqrt{\gamma^2 - \lambda(\gamma^2 - 1)} V_C \quad (26)$$

By substituting (26) into (22),

$$\begin{aligned} v_d(t_{h1}) &= V_C + \mu \sqrt{\lambda + (1 - \lambda) \gamma^2} V_C - v_{DC}(0) \\ &= [1 + \mu \sqrt{\gamma^2 - \lambda(\gamma^2 - 1)} - \mu \gamma] V_C \end{aligned} \quad (27)$$

### 3. Stage II [ $t_{h1}$ , $t_{h2}$ ]

In this stage, the capacitors  $C$  and  $C_{DC}$  are connected in series. At  $t_{h2}$ , the output voltage  $v_d(t_{h2}) = V_{d,\min} = \rho V_C$ . The final voltages across  $C$  and  $C_{DC}$  can be expressed as

$$\begin{aligned} \Delta v_C(t_{h2}) &= \Delta v_C(t_{h1}) + \frac{C_a}{C_a + C} [v_d(t_{h1}) - v_d(t_{h2})] \\ &= \Delta v_C(t_{h1}) + \Delta x V_C \end{aligned} \quad (28)$$

$$\begin{aligned} v_{DC}(t_{h2}) &= v_{DC}(t_{h1}) - \frac{C}{C_a + C} [v_d(t_{h1}) - v_d(t_{h2})] \\ &= \Delta v_C(t_{h1}) - \lambda \Delta x V_C \end{aligned} \quad (29)$$

where  $\Delta x = \frac{1}{1 + \lambda} \{ (1 - \rho) - \mu [\gamma - \sqrt{\gamma^2 - \lambda(\gamma^2 - 1)}] \}$ .

By applying the conservation of energy,

$$\frac{1}{2} C v_C^2(t_{h1}) + \frac{1}{2} C_{DC} v_{DC}^2(t_{h1}) - \frac{1}{2} C v_C^2(t_{h2}) - \frac{1}{2} C_{DC} v_{DC}^2(t_{h2}) = P_L (t_{h2} - t_{h1}) \quad (30)$$

It can be derived from (30) that

$$t_{h2} - t_{h1} = \frac{\beta}{\omega} \left( \frac{\rho}{\mu} \Delta x + \frac{1 + \lambda}{2 \mu} \Delta x^2 \right) \quad (31)$$

Based on (24) and (31), the hold-up time  $t_h$  and the number of hold-up cycle  $N$  are

$$t_h = \frac{\beta}{\omega} \left( \frac{\rho}{\mu} \Delta x + \frac{1+\lambda}{2\mu} \Delta x^2 + \gamma - 1 \right) \quad (32)$$

$$N = \frac{\beta}{2\pi} \left( \frac{\rho}{\mu} \Delta x + \frac{1+\lambda}{2\mu} \Delta x^2 + \gamma - 1 \right) \quad (33)$$

The hold-up time of the dc-link with only a capacitor bank storing the same amount of energy is derived as follows. Let the corresponding dc-link capacitance required, the hold-up time and hold-up cycle be  $C'$ ,  $t_h'$ , and  $N'$  respectively. Thus, for the same amount of energy stored in  $C'$  as with the dc-link module,

$$C' = \frac{C V_C^2 + C_{DC} v_{DC}^2(0)}{V_C^2} = \left( 1 + \frac{\gamma^2 \mu^2}{\lambda} \right) C \quad (34)$$

By assuming that the ripple currents following through the dc-link capacitors with and without the voltage compensator are the same,

$$\mu' = \frac{\Delta v_C'}{V_C} = \frac{\beta I_D}{\omega C' V_C} \quad (35)$$

Hence, by using (34) and (35),

$$\begin{aligned} t_h' &= \frac{C' [V_C - \Delta v_C(0)]^2 - C' (\rho V_C)^2}{2 P_L} \\ &= \frac{\beta}{\omega} \frac{(\lambda + \gamma^2 \mu^2) \left[ \left( 1 - \frac{\lambda \mu}{\lambda + \gamma^2 \mu^2} \right)^2 - \rho^2 \right]}{2 \lambda \mu} \end{aligned} \quad (36)$$

$$N' = \frac{\beta}{2\pi} \frac{(\lambda + \gamma^2 \mu^2) \left[ \left( 1 - \frac{\lambda \mu}{\lambda + \gamma^2 \mu^2} \right)^2 - \rho^2 \right]}{2 \lambda \mu} \quad (37)$$

Equations (32), (33), (36) and (37) will be used to compare the hold-up time with and without the proposed dc-link module. The design guidelines will be given in the next section.

#### IV. Design Guidelines for the DC-link Module

The design guidelines for applications with and without hold-up time requirements are given below.

##### A. Applications without hold-up time requirement

Some applications, like electronic ballasts, do not have the hold-up time requirement. The dc-link module is used to balance the input and output power difference, and reduce the dc-link voltage ripple. Fig. 5 shows the energy storage  $E$  and instantaneous power  $p$  of the dc-link capacitor. The dc component of energy  $E_1$  maintains a certain level of dc-link voltage. Only the ac component of  $E$  requires the power  $p$  for balancing the input and output power of the entire system. Therefore, with the proposed dc-link module, the energy storage elements are divided into two parts: one is stored in the reduced dc-link capacitor and the other one is stored in the voltage compensator. The theoretical minimum energy storage required is  $E_{\min}$ . In the practical design, the overall energy storage of the dc-link module is reduced to a certain level between  $E_1$  and  $E_{\min}$ , for example  $E_2$  as illustrated in Fig. 5.

The reduction of the dc-link capacitance is limited by the voltage stresses on the dc source capacitor and switching devices in the module. Assume that the load current  $i_d$  is constant in the module. Based on (5), the dc-link capacitor current  $i_c$  equals  $\Delta i_a$ . Thus,

$$i_c = C \frac{dv_c}{dt} = \Delta i_a \Rightarrow C |\Delta v_c| = \text{constant} \quad (38)$$

The product of the dc-link capacitance and its peak ripple voltage is a constant. Thus, the minimum value of  $v_{DC}$  equals  $|\Delta v_c|$ . Fig. 6 shows the relationship between the value of  $C$  and  $v_{DC}$ . Without the dc-link module, it requires a capacitance of  $C_{norm}$  for meeting the design

specification. Practically, the chosen value for  $C$  is larger than  $C_{norm}$  in order to sustain the ripple current stress. Due to the aging effect of the capacitor changing from  $C_{norm}$  to  $C_{norm}'$ , the peak-to-peak dc-link voltage ripple will increase from  $2|\Delta v_{C,norm}|$  to  $2|\Delta v_{C,norm}'|$ .

The design of the dc-link capacitance value  $C$  with the dc-link module is a compromise among the allowable voltage level of  $v_{DC}$ , and the stress on the capacitor  $C_{DC}$  and the MOSFETs  $S_1 - S_4$ . A smaller value of  $C$  requires higher voltage ratings of  $C_{DC}$  and  $S_1 - S_4$ . Moreover, a boundary capacitance  $C_{bd}$  can be determined based on specifications of power electronic systems, availability, cost and volume of different type of capacitors. It provides a guideline on the selection of capacitor type. For instance, power film capacitors can be applied in *Choice 1* with a higher dc voltage on  $C_{DC}, V_{DC,1}$ , as compared to that of *Choice 2* with lower voltage  $V_{DC,2}$  in which E-Caps are used. Thus, with the aid of the dc-link module, the required dc-link capacitance can be reduced, making it possible to use capacitor of long lifetime, like power film capacitors, to ensure the lifetime of the entire power electronic system, or extend the performance lifetime even if there is a significant reduction in the capacitance of the dc-link capacitor due to the aging effect.

The value of  $C_{DC}$  is determined by using (17) to limit the voltage ripple of  $v_d$ . In the application example (a power factor corrector (PFC) front-end stage plus a dc-dc converter) discussed in Section V, with conventional E-Cap solution (without the voltage compensator),

$$2|\Delta v_C| = \frac{2I_D}{\omega_1 C_{norm}} \quad (39)$$

According to (17) and (39), as  $m_{a1} \leq 1$ , the voltage ripple across the output terminal of the dc-link module can be limited to lower than the one with conventional E-Cap solution by choosing

$C_{DC}$  no less than half of the capacitance of the E-Cap, that is

$$C_{DC} \geq \frac{1}{2} C_{norm} \quad (40)$$

As the capacitor  $C_{DC}$  withstands a low voltage stress, there are several choices in practical implementation. One choice is to use low voltage E-Caps with high ripple current and long lifetime. Unlike the ones with high voltage ratings, they are available and cost-effective. Another choice is to use ceramic capacitor tank or low-voltage film capacitors.

#### B. Applications with hold-up time requirement

For this type of applications, the determining factor for the energy storage is the required hold-up time rather than the voltage ripple specification. The design guidelines discussed are based on the analysis in Sec. III.

Figs. 7 and 8 show the graphical representations of equations (33) and (37) with  $\beta = 1$  (the amplitude of the dc link capacitor ripple current is equal to the value of the average load current),  $\rho = 0.8$  ( $V_{d,min}$  is 80% of the dc-link voltage prior to the supply outage), and  $\mu = 0.02$  (dc link ripple voltage is 2% of the average dc-link voltage). It should be noted in the comparison that the factors  $\lambda$  and  $\gamma$  are for the proposed dc-link module containing an additional energy storage capacitor  $C_{DC}$ . They appear in (37) as the comparison is based on the same energy storage. As depicted in Fig. 7, with proper choices of  $\lambda$  (ratio between  $C$  and  $C_{DC}$ ) and  $\gamma$  (ratio between  $v_{DC}$  and  $|\Delta v_C|$ ), the number of hold-up cycles with the dc-link module can be increased. The shaded area of the  $\lambda$  -  $\gamma$  selection curves shown in Fig. 8 represents an extended hold-up time (i.e.,  $N / N' > 1$ ). That means, with the same amount of energy storage in the dc link, the hold-up time with the dc-link module is longer than using a dc-link capacitor only.

Different curves showing the constant number of the hold-up cycles and  $N / N'$  ratios are plotted in dot lines and solid lines, respectively.

The illustrations given in Fig. 7 and Fig. 8 are with  $\mu = 0.02$ , which is corresponding to a determined value of the dc-link capacitance  $C$  from the design perspective. Therefore, the trade-off design condition is between maximization of  $N / N'$  and minimization of  $C_{DC}$  and its voltage stress  $v_{DC}$ , meanwhile, achieving the required hold-up cycle  $N$ . Different figures can be plotted for other values of  $\mu$ , corresponding to different values of  $C$ . By considering all of the values of  $\lambda$  and  $\gamma$  selected for different value of  $\mu$ , it allows the selection of the optimal values of  $\mu$ ,  $\lambda$  and  $\gamma$ . Thus, the optimal values of  $C$ ,  $C_{DC}$ , and  $v_{DC}$  are selected.

## V. Experimental Verifications

An experimental ac-dc-dc converter test bed as shown in Fig. 9(a) has been built. It is constructed by connecting a 3kW PFC - STMicroelectronics STEVAL-ISF001V1 to a 600W phase-shifted full-bridge dc-dc converter - Texas Instruments UCC28950EVM-442. An input LC filter composed of 1.47 $\mu$ F film capacitors (1 $\mu$ F and 0.47 $\mu$ F in parallel) and a 20 $\mu$ H inductor is applied to smooth the input current  $i_d$ . The detailed circuit and operation of the phase-shifted full-bridge dc-dc converter are discussed in [30] except for that the 330 $\mu$ F input capacitor in the evaluation board is removed in the experiments. The PFC is supplied by an AC power source Kikusui PCR2000LA. The supply voltage is 220V, 50Hz. The output of the dc-dc converter is connected to an electronic load Kikusui PLZ1003W. The rated output voltage of the dc-dc converter is 12V. The output capacitor bank  $C$  in the PFC is formed by connecting two 330 $\mu$ F, 450V E-Cap capacitors in parallel. According to the manufacturer's datasheet, the lifetime of the

capacitors is 3,000 hours at 105°C (12,000 hours estimated at 85°C and rated ripple current). Figs. 10(a) and (b) show the startup transient and steady-state waveform of  $v_C$  when the output is full load. The average dc voltage is 400V and peak-to-peak ac ripple voltage (i.e.,  $\Delta v_C$ ) is 10.8V. The settling time of the startup process is 150ms. Fig. 10(c) shows the output current  $i_{out}$  and  $v_C$  when the output is suddenly changed from 10% load to full load.  $v_C$  is momentarily dropped by 45V and the settling time is 100ms. Fig. 10(d) shows the corresponding waveforms when the output is suddenly changed from full load to 10% load.  $v_C$  is momentarily jumped up by 37.7V and the settling time is 150ms. Fig. 10(e) shows the waveforms of  $v_C$ , PFC input voltage  $v_s$  and output current  $i_{out}$  when  $v_s$  is suddenly turned off.  $v_C$  reduces to 320V (80% of 400V) after 24.6ms. Within this period, the dc-dc converter is still in normal operation. The measured steady-state RMS value of capacitor current and ESR of the capacitor bank is 1.7A and 130mΩ, respectively. Thus, the total power loss of the capacitor bank is estimated to be 0.38W at full load.

The E-Cap bank is replaced by the proposed module. The circuit schematic of the module is shown in Fig. 9(b). The power stage design of the voltage compensator follows the way to design a typical full-bridge inverter as discussed in [29]. The input voltage level of the voltage compensator is selected according to the dc-link capacitance (as shown in Fig. 6) and the modulation index of the SPWM controller. In the prototype, the modulation index is 0.5 under full load condition to achieve a sufficient robustness margin and avoid over modulation. The dc-link capacitance is 120μF (in the case without hold-up time requirement) with a peak-to-peak voltage ripple of about 50V. Thus, the input voltage  $v_{DC}$  is regulated at 50V by setting a 5V reference in the control stage. The switching frequency of the voltage compensator is 50 kHz.



Components used in the power conversion stage and the key design parameters are listed in Table I. Two design cases are investigated. The first design has no hold-up time requirement while the second one has the hold-up requirement. They are discussed as follows.

*A. Without hold-up time requirement*

A 120 $\mu$ F (82% capacitance reduction) film capacitor with the lifetime of 100,000 hours at 85°C and rated ripple current is used to replace the capacitor bank. A 1000 $\mu$ F, 63V low-voltage E-Cap with the lifetime of 8,000 hours at 125°C (128,000 hours estimated at 85°C and rated ripple current, which is comparable with the lifetime of the film capacitor) is used for the module, i.e.  $C_{DC}$ . The voltage across  $C_{DC}$  is designed to be 50V. Fig. 11(a) shows the startup transient of the module output  $v_d$ . The dc value of  $v_d$  is 400V. The settling time of the startup process is 75ms. Fig. 11(b) shows the steady-state waveforms of the capacitor ripple voltage  $\Delta v_C$  and module output ripple voltage  $\Delta v_d$ , when the output is at full load. Their peak-to-peak ripple voltages are 49.1V and 3.9V, respectively. Figs. 11(c) and (d) show the transient waveforms of  $v_d$ ,  $v_C$ , module output voltage  $v_{ab}$ , input current of the full-bridge dc-dc converter  $i_d$ , output voltage of the dc-dc converter  $v_{out}$  and output current of the dc-dc converter  $i_{out}$ , when the output is suddenly changed from 10% load to full load.  $v_d$  is momentarily reduced by 45.5V and its settling time is 100ms. Figs. 11(e) and (f) show the corresponding waveforms when the output is suddenly changed from full load to no load.  $v_d$  is momentarily increased by 37.7V and its settling time is 150ms. Compared Fig. 10(a) with Fig. 11(a), and Fig. 10(b) with Fig. 11(b), the startup time is shorter and the ripple voltage is smaller with the proposed module. As shown in Figs. 10(c) and (d), and Figs. 11(c) and (e), under the load change conditions, the transient

responses of the system with the module are similar to the ones with the E-Cap bank. The total power dissipation of the module is around 1.5W. From the perspective of the capacitor lifetime at 85°C with a same ripple current design margin, the proposed module is estimated to have a lifetime more than eight times of that of the E-Caps without the voltage compensator.

#### *B. With hold-up time requirement*

The module is designed to achieve the same hold-up time with the electrolytic capacitors. Based on the design method described in Section IV, a 450μF capacitor (32% capacitance reduction) is used for  $C$  and a 1000μF, 63V low-voltage electrolytic capacitors for  $C_{DC}$ , corresponding to an overall energy storage of 72% of that with E-Caps solution without the voltage compensator. Fig. 11(g) shows the waveforms of  $v_d$ ,  $v_s$ ,  $v_{ab}$ , and  $i_{out}$  after  $v_s$  is suddenly turned off under the full load condition. Compared Fig. 10(e) with Fig. 11(g), the proposed module gives a similar hold-up performance to the electrolytic capacitor bank with 28% energy storage reduction.

Thus, the experimental results reveal that the proposed dc-link module can reduce the required capacitance value for the dc-link capacitor without sacrificing the transient and steady-state responses of the whole system. Although the proposed module requires capacitors as the dc source, the voltage level is only 50V, allowing the use of low-voltage capacitors of long lifetime. The only drawback is that there is an increase in the overall power loss by 1.12W.

From the practical point of view, the use of E-Caps is still the low-cost solution. Then, even if the E-Cap bank is unchanged in the application, the proposed module allows a wide range of reduction in the dc-link capacitance (due to aging effect) without sacrificing the performance. For applications without the hold-up requirement, it allows the reduction of the dc-

link capacitance from  $660\mu\text{F}$  to  $120\mu\text{F}$  in the test. For applications with the hold-up time requirement, the module allows the reduction from  $660\mu\text{F}$  to  $450\mu\text{F}$  and 28% reduction of the overall energy storage in the dc-link module. The resulting effect will extend the life expectancy of the entire system from the perspective of reducing the chance of system failure due to aging of the dc link capacitors. The proposed method has a distinct advantage for high-voltage applications, due to the fact that the voltage rating of power film capacitors is usually higher than that of E-Caps. With the proposed module, the dc-link capacitance can be reduced and a fewer number of high-voltage power film capacitors are used to replace the E-Caps.

## VI. Conclusions

An active series voltage compensator for reducing the dc-link capacitance in a capacitor-supported power electronic system has been proposed. The implementation requires low-voltage devices only, as the dc-link module only handles ripple voltage on the dc-link and reactive power flow between in the dc-link. A detailed study on the dc and ac characteristics, stability analysis, and hold-up time performance has been given. The design guidelines for the dc-link module for applications with and without the hold-up time requirement have been described. The proposed method has been demonstrated on a two-converter system with the front-stage power factor corrector and second-stage of dc-dc converter. The performances with the capacitor bank only and the proposed dc-link module have also been compared.

## Appendix

### A. *Proof of Equation (6)*

Based on equations (4) and (5), equation (6) is derived as follows:

$$\begin{aligned}
P_{ab} &= \frac{1}{T} \int_0^T v_{ab}(t) [\Delta i_d(t) + I_D] dt \\
&= \frac{1}{T} \int_0^T v_{ab}(t) \Delta i_d(t) dt + 0 \\
&= \frac{1}{T} \int_0^T \left[ \frac{|\Delta I_a|}{\omega_1 C} \sin(\omega_1 t + \delta_1 - 90^\circ) - \frac{|\Delta I_d|}{\omega_2 C} \sin(\omega_2 t + \delta_2 - 90^\circ) \right] |\Delta I_d| \sin(\omega_2 t + \delta_2) dt \\
&= \frac{|\Delta I_d| \|\Delta I_a\|}{2 \omega_1 C T} \int_0^T \{ \sin[(\omega_1 - \omega_2)t + (\delta_1 - \delta_2)] - \sin[(\omega_1 + \omega_2)t + (\delta_1 + \delta_2)] \} dt - 0 \\
&= \frac{|\Delta I_d| \|\Delta I_a\|}{2 \omega_1 C T} \int_0^T \sin[(\omega_1 - \omega_2)t + (\delta_1 - \delta_2)] dt - \frac{|\Delta I_d| \|\Delta I_a\|}{2 \omega_1 C T} \int_0^T \sin[(\omega_1 + \omega_2)t + (\delta_1 + \delta_2)] dt \\
&= \frac{|\Delta I_d| \|\Delta I_a\|}{2 \omega_1 C T} \int_0^T \sin[(\omega_1 - \omega_2)t + (\delta_1 - \delta_2)] dt - 0 \\
&= \frac{|\Delta I_d| \|\Delta I_a\|}{2 \omega_1 C T} \int_0^T \sin[(\omega_1 - \omega_2)t + (\delta_1 - \delta_2)] dt
\end{aligned}$$

## References

- [1] G. Terzulli, "Film technology to replace electrolytic technology in wind power applications," AVX Technical Note, 2010.
- [2] EPCOS, "Film capacitors for industrial applications," Product Profile, Edition 04.07, 2007.
- [3] X. Chen, and M. Kazerani, "Space vector modulation control of an AC-DC-AC converter with a front-end diode rectifier and reduced DC-link capacitor," *IEEE Trans. Power Electron.*, vol. 21, no. 5, pp. 1470-1478, Sep., 2006.
- [4] C. R. Neuhaus, and R. W. D. Doncker, "DC-link voltage control for switched reluctance drives with reduced DC-link capacitance," in *Proc. IEEE Energy Convers. Congr. and Expo.*, 2010, pp. 4192-4198.
- [5] D. Lamar, J. Sebastian, M. Arias, and A. Fernandez, "On the limit of the output capacitor reduction in power-factor correctors by distorting the line input current," *IEEE Trans. Power Electron.*, vol. 27, no. 3, pp. 1168-1176, Mar. 2012.

- [6] P. Pelletier, J. M. Guichon, J. L. Schanen, and D. Frey, "Optimization of a DC capacitor tank," *IEEE Trans. Ind. Appl.*, vol. 45, no. 2, pp. 880-886, Mar./Apr., 2009.
- [7] P. W. Hammond, "Control method and apparatus to reduce current through DC capacitor linking two static converters," U.S. Patent 6,762, 947, Jul. 13, 2004.
- [8] G. Kalman, and C. Huggett, "AC-to-AC power converter without a DC link capacitor," U.S. Patent 6,839,249, Jan. 4, 2005.
- [9] B. G. Gu, and K. Nam, "A DC-link capacitor minimization method through direct capacitor current control," *IEEE Trans. Ind. Appl.*, vol. 42, no. 2, pp. 573-581, Mar./Apr., 2006.
- [10] I. S. Freitas, C. B. Jacobina, and E. C. Santos, "Single-phase to single-phase full-bridge converter operating with reduced AC power in the DC-link capacitor," *IEEE Trans. Power Electron.*, vol. 25, no. 2, pp. 272-279, Feb., 2010.
- [11] T. Okuda, T. Urakabe, and Y. Kuramoto, "Motor driving apparatus," U.S. Patent 7, 310, 475, Dec. 18, 2007.
- [12] H. Song, D. Oh, K. Nam, and S. Kim, "Method for controlling voltage of DC-link for electric vehicle," U.S. Patent 7,528,566, May 5, 2009.
- [13] J. Ying, Q. Zhang, A. Qiu, T. Liu, X. Guo, and J. Zeng, "DC-DC converter circuits and method for reducing DC-bus capacitor current," U.S. Patent 7,009,852, Mar. 7, 2006.
- [14] D. C. Hamill, and P. T. Krein, "A 'zero' ripple technique applicable to any DC Converter," *in Proc. IEEE Power Electron. Spec. Conf.*, 1999, pp. 1165-1171.
- [15] B. K. Bose, and D. Kastha, "Electrolytic capacitor elimination in power electronic system by high frequency active filter," *in Proc. Ind. Appl. Soc. Annu. Meeting*, 1991, pp. 869-878.
- [16] P. E. Nuechterlein, "DC-link ripple reduction circuit," U.S. Patent 5,014,177, May 7, 1991.
- [17] Y. Wang, G. Joos, and H. Jin, "DC-side shunt-active power filter for phase-controlled

- magnet-load power supplies,” *IEEE Trans. Power Electron.*, vol. 12, no. 5, pp. 765-771, Sep. 1997.
- [18] T. Shimizu, Y. Jin, and G. Kimura, “DC ripple current reduction on a single-phase PWM voltage-source rectifier,” *IEEE Trans. Ind. Appl.*, vol. 36, no. 5, pp. 1419-1429, Sep./Oct. 2000.
- [19] O. Garcia, M. D. Martinez-Avial, J. A. Cobos, J. Uceda, J. Gonzalez, and J. A. Navas, “Harmonic reducer converter,” *IEEE Trans. Ind. Electron.* vol. 50, no. 2, pp. 322-327, Apr. 2003.
- [20] D. Zhou, “Reduced capacitance AC/DC/AC power converter,” U.S. Patent 6,804,127, Oct. 12, 2004.
- [21] C. Kyritsis, N. P. Papanicolaou, and E. C. Tatakis, “A novel parallel active filter for current pulsation smoothing on single stage grid-connected AC-PV modules,” in *Proc. European Conf. on Power Electron. and Appl.*, 2007, pp. 1-10.
- [22] S. G. Li, B. Ozpineci, and L. M. Tolbert, “Evaluation of a current source active power filter to reduce the DC bus capacitor in a hybrid electric vehicle traction drive,” in *Proc. IEEE Energy Convers. Congr. and Expo.*, 2009, pp. 1185-1190.
- [23] H. Yoo, and S. K. Sul, “A new circuit design and control to reduce input harmonic current for a three-phase AC machine drive system having a very small DC-link capacitor,” in *IEEE Appl. Power Electron. Conf.*, 2010, pp. 611-618.
- [24] R. X. Wang, F. Wang, D. Boroyevich, R. Burgos, R. X. Lai, P. Q. Ning, and K. Rajashekara, “A high power density single-phase PWM rectifier with active ripple energy storage,” *IEEE Trans. Power Electron.*, vol. 26, no. 5, pp. 1430-1443, May 2011.
- [25] H. B. Li, K. Zhang, and H. Zhao, “Active DC-link power filter for single phase PWM

- rectifiers,” in *Proc. IEEE Int. Conf. on Power Electron. and ECCE Asia*, 2011, pp. 2920-2926.
- [26] X. Du, L. W. Zhou, H. Lu, and L. M. Tai, “DC link active power filter for three-phase diode rectifier,” *IEEE Trans. Ind. Electron.*, vol. 59, no. 3, pp. 1430-1442, Mar. 2012.
- [27] P. Krein, R. Balog, and M. Mirjafari, “Minimum energy and capacitance requirements for single-phase inverters and rectifiers using a ripple port,” *IEEE Trans. Power Electron.*, vol. 27, no. 11, pp. 4690-4698, Nov. 2012.
- [28] H. Hu, S. Harb, N. H. Kutkut, Z. J. Shen, and I. Batarseh, “A single-state microinverter without using electrolytic capacitors,” *IEEE Trans. Power Electron.*, vol. 28, no. 6, pp. 2677-2687, Jun. 2013.
- [29] N. Mohan, T. M. Undeland, and W. P. Robbins, *Power Electronics, Converters, Applications, and Design*, John Wiley & Sons Press, 2003, ch8.
- [30] Texas Instruments User’s Guide SLUU421A, *600-W phase-shifted full-bridge converter*, May 2010.

## Footnotes

Manuscript received ...

The work described in this paper was fully supported by a grant from the Research Grants Council of the Hong Kong Special Administrative Region, China (Project No.: CityU 112512).

Preliminary partial results of this research have been presented at the *IEEE Energy Conversion Congress and Exposition 2011, Phoenix, Arizona, USA*, the *IEEE Applied Power Electronics Conference and Exposition 2012, Orlando, Florida, USA*, and *IEEE Energy Conversion Congress and Exposition 2012, Raleigh, North Carolina, USA*.

\* The author is with the Center of Reliable Power Electronics (CORPE), Department of Energy Technology, Aalborg University, Pontoppidanstraede 101, DK-9220 Aalborg, Denmark.

† The authors are with the Centre for Smart Energy Conversion and Utilization Research (CSCR), City University of Hong Kong, Tat Chee Avenue, Kowloon Tong, Kowloon, Hong Kong.



### Figure captions

- Fig. 1 Basic concept of the proposed dc-link module.
- Fig. 2 Control mechanism with a capacitor as the input source of the voltage compensator.
- Fig. 3 Operation timing diagram of the voltage compensator.
- Fig. 4 Operations during the hold-up time. (a) Waveforms. (b) Circuit during the time interval  $[0, t_{h1}]$ . (c) Circuit during the time interval  $[t_{h1}, t_{h2}]$ .
- Fig. 5 Energy stored and instantaneous power handled by the dc-link capacitor.
- Fig. 6 Relationship between the dc-link capacitance, ripple voltage, and  $v_{DC}$ .
- Fig. 7 Hold-up time analysis with and without the dc-link module ( $\beta = 1$ ,  $\rho = 0.8$ ,  $\mu = 0.02$ ).
- Fig. 8 Design curves for selection of  $\lambda$  and  $\gamma$  ( $\rho = 0.8$ ,  $\mu = 0.02$ ).
- Fig. 9 Experimental test bed. (a) System configuration. (b) Circuit schematic of the proposed module.
- Fig. 10 Experimental waveforms with an electrolytic capacitor bank. (a) Startup transient under the full load condition ( $v_C$ : 100V/div, Timebase: 50ms/div). (b) Steady-state dc-link voltage waveform under the full load condition ( $\Delta v_C$ : 2V/div, Timebase: 10ms/div). (c) Transient waveforms when the output is changed from 10% load to full load ( $v_C$ : 100V/div,  $i_{out}$ : 50A/div, Timebase: 50ms/div). (d) Transient waveforms when the output is changed from full load to 10% load. ( $v_C$ : 100V/div,  $i_{out}$ : 50A/div, Timebase: 50ms/div). (e) Transient waveforms after a sudden supply outage under the full-load condition. ( $v_C$ : 100V/div,  $v_S$ : 300V/div,  $i_{out}$ : 20A/div, Timebase: 10ms/div).
- Fig. 11 Experimental waveforms with the proposed dc-link module. (a) Start-up transient under the full load condition. ( $v_d$ : 100V/div, Timebase: 50ms/div). (b) Steady-state

waveforms of  $v_C$  and  $v_d$  under the full load condition ( $\Delta v_C$ : 20V/div,  $\Delta v_d$ : 2V/div, Timebase: 10ms/div). (c) Transient waveforms of the dc-link module when the output is changed from 10% load to full load ( $v_d$ : 100V/div,  $v_C$ : 100V/div,  $v_{ab}$ : 40V/div,  $i_d$ : 2A/div, Timebase: 50ms/div). (d) Transient waveforms of the full-bridge dc-dc converter when the output is changed from 10% load to full load ( $v_d$ : 100V/div,  $i_d$ : 2A/div,  $v_{out}$ : 10V/div,  $i_{out}$ : 50A/div, Timebase: 50ms/div). (e) Transient waveforms of the dc-link module when the output is changed from full load to 10% load ( $v_d$ : 100V/div,  $v_C$ : 100V/div,  $v_{ab}$ : 40V/div,  $i_d$ : 2A/div, Timebase: 50ms/div). (f) Transient waveforms of the full-bridge dc-dc converter when the output is changed from full load to 10% load ( $v_d$ : 100V/div,  $i_d$ : 2A/div,  $v_{out}$ : 10V/div,  $i_{out}$ : 50A/div, Timebase: 50ms/div). (g) Transient waveforms after a sudden supply outage under the full-load condition ( $v_d$ : 100V/div,  $v_S$ : 300V/div,  $v_{ab}$ : 20V/div,  $i_{out}$ : 50A/div, Timebase: 10ms/div).

### Table captions

Table I Values of the components used in the module

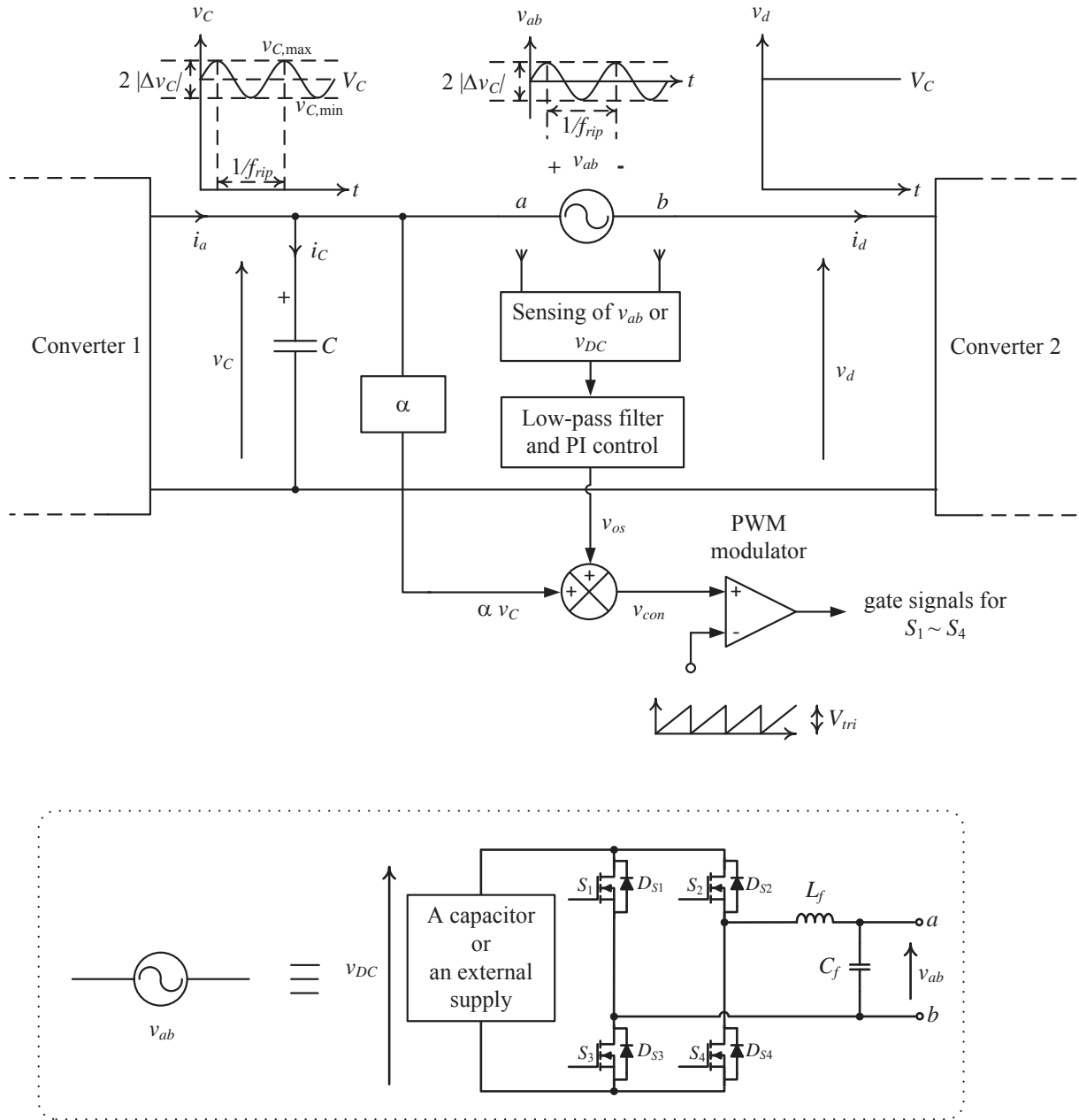


Fig. 1 Basic concept of the proposed dc-link module.

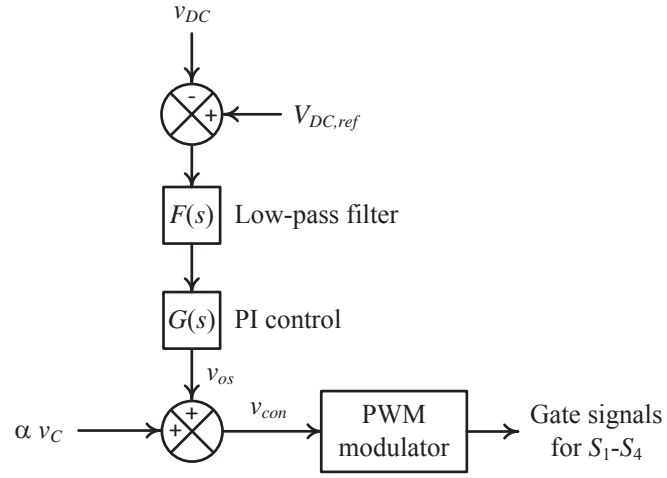


Fig. 2 Control mechanism with a capacitor as the input source of the voltage compensator.

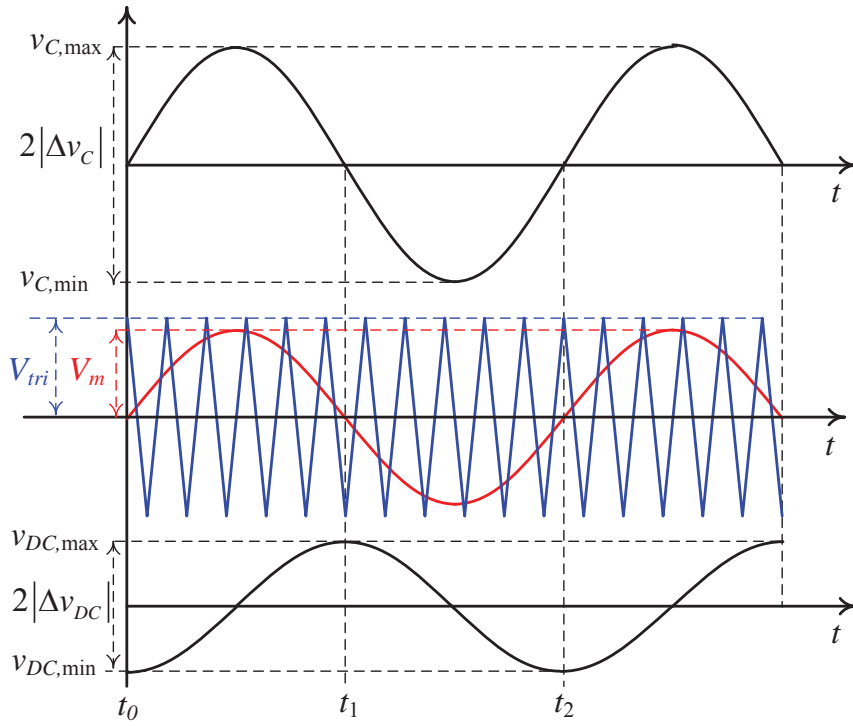
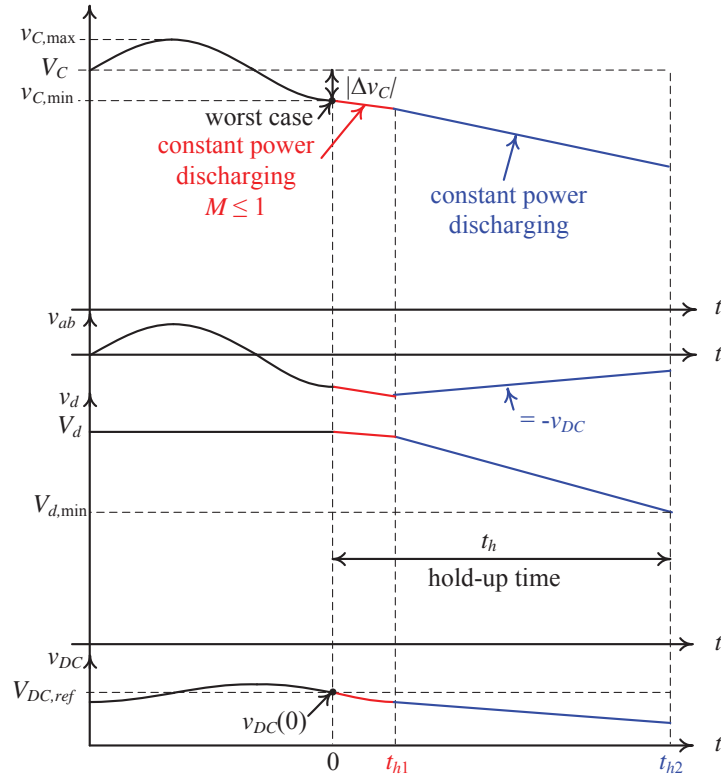
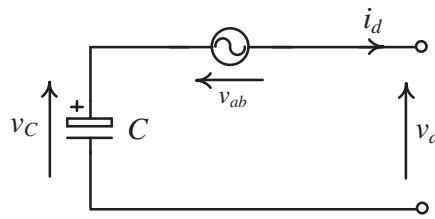


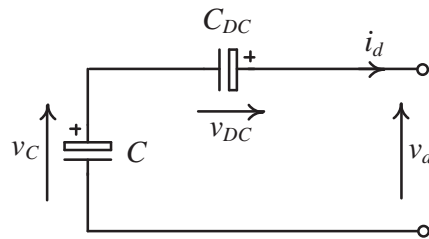
Fig. 3 Operation timing diagram of the voltage compensator.



(a) Waveforms.



(b) Circuit during the time interval  $[0, t_{h1}]$ .



(c) Circuit during the time interval  $[t_{h1}, t_{h2}]$ .

Fig. 4 Operations during the hold-up time.

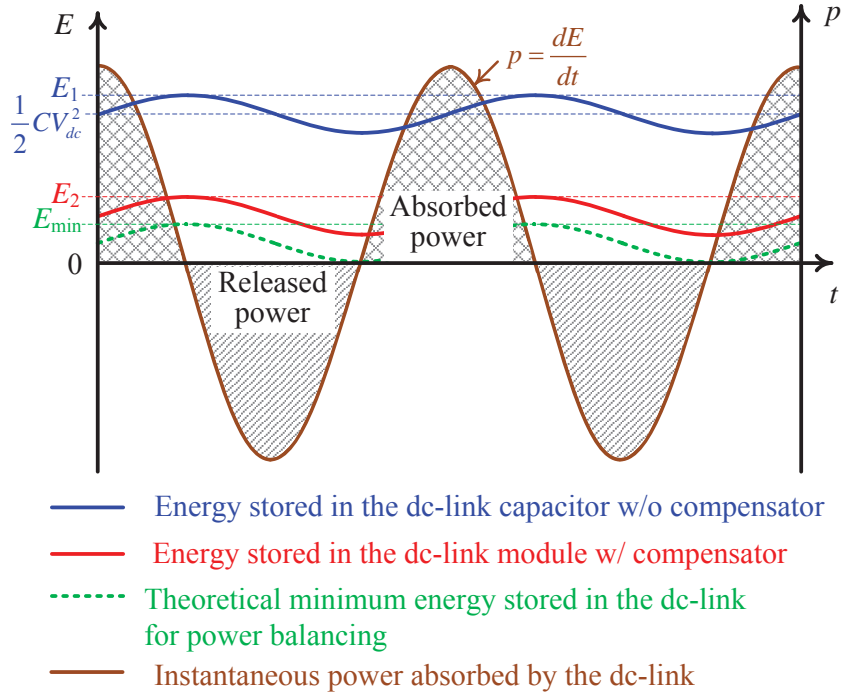


Fig. 5 Energy stored and instantaneous power handled by the dc-link capacitor.

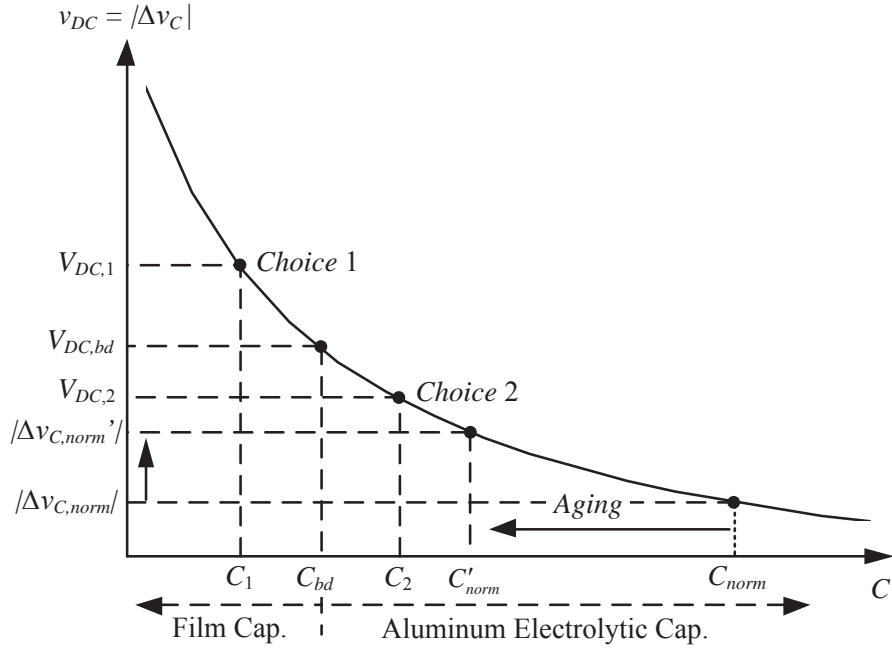


Fig. 6 Relationship between the dc-link capacitance, ripple voltage, and  $v_{DC}$ .

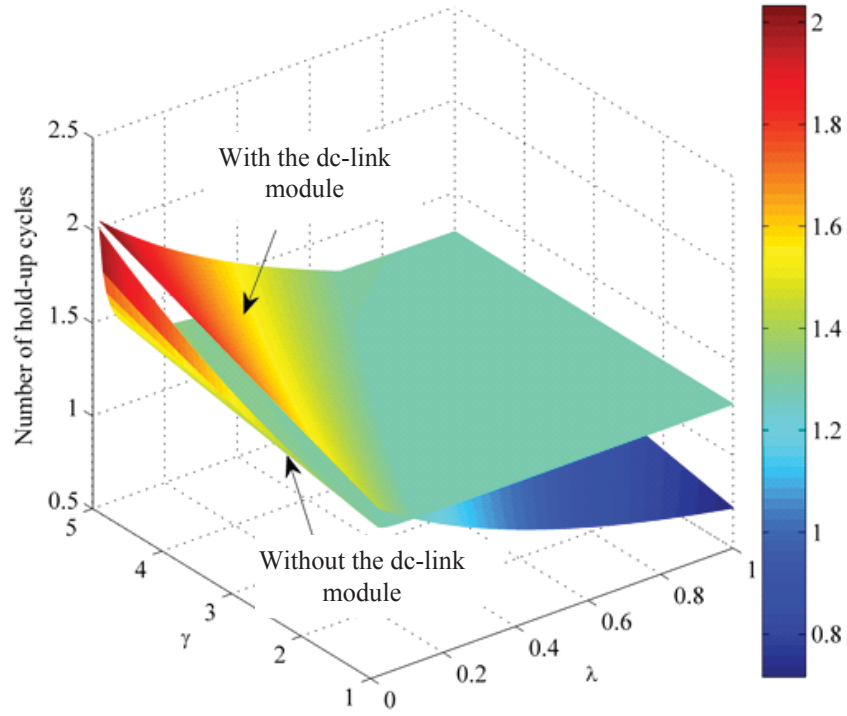


Fig. 7 Hold-up time analysis with and without the dc-link module ( $\beta = 1$ ,  $\rho = 0.8$ ,  $\mu = 0.02$ ).

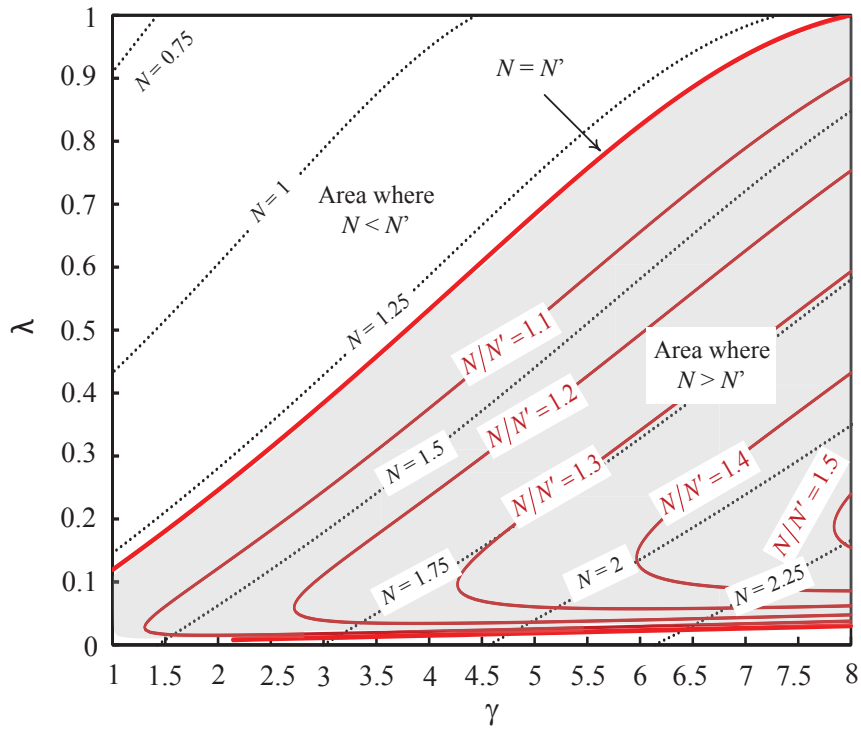
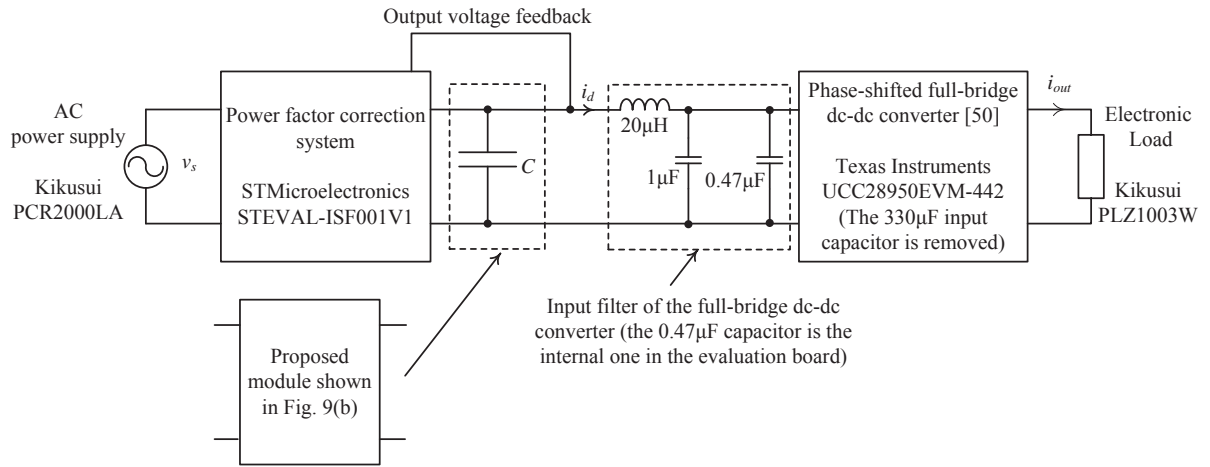
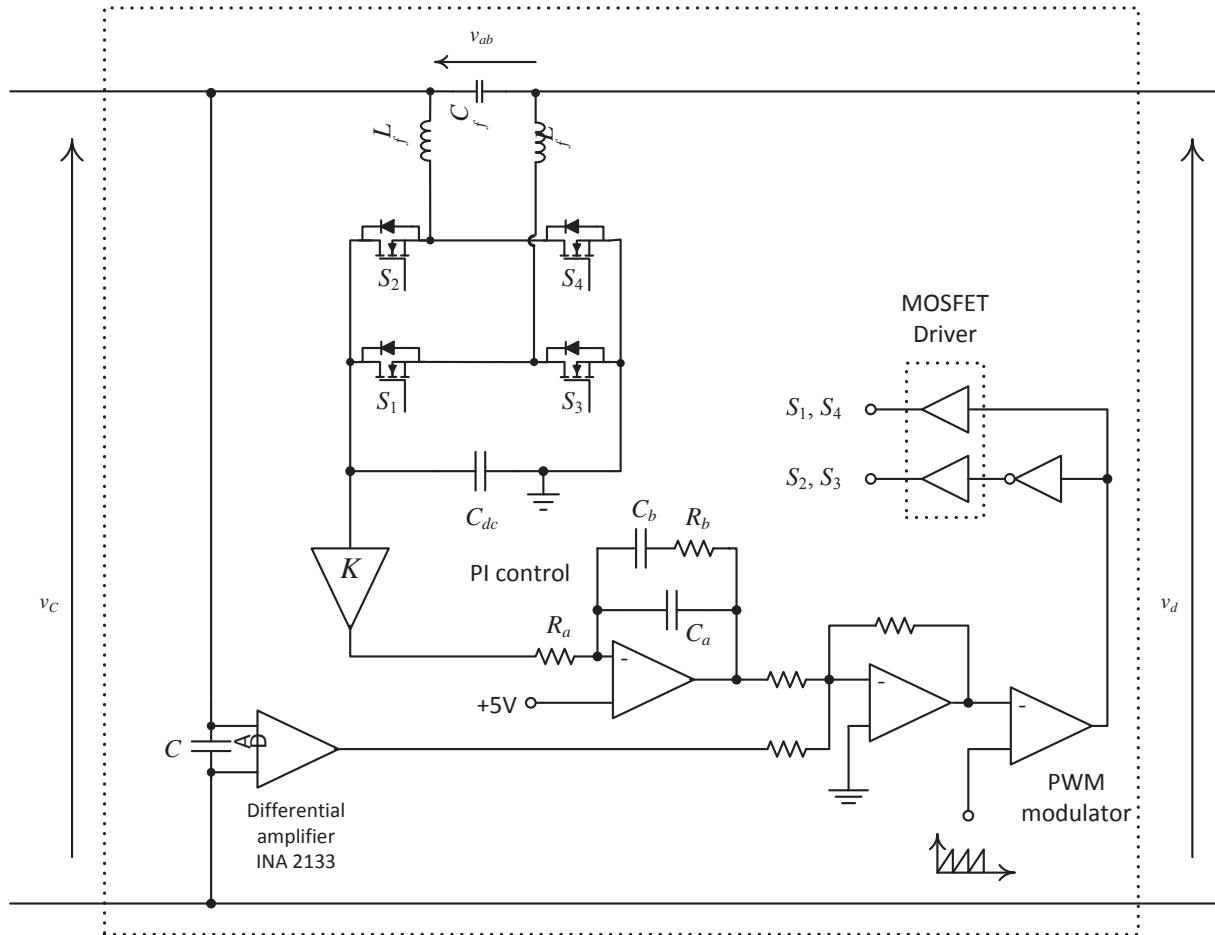


Fig. 8 Design curves for selection of  $\lambda$  and  $\gamma$  ( $\rho = 0.8$ ,  $\mu = 0.02$ ).



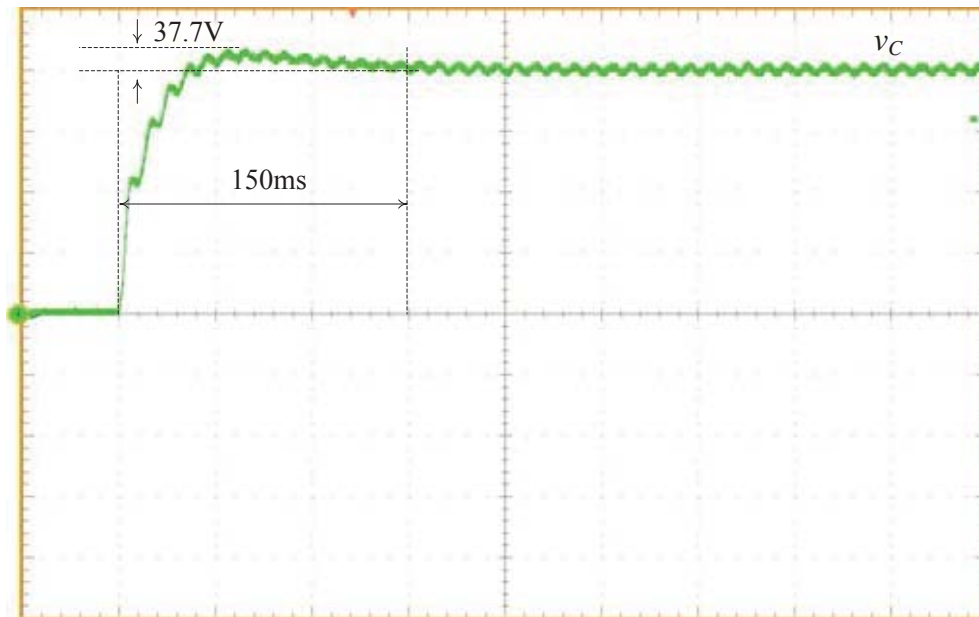
(a) System configuration.



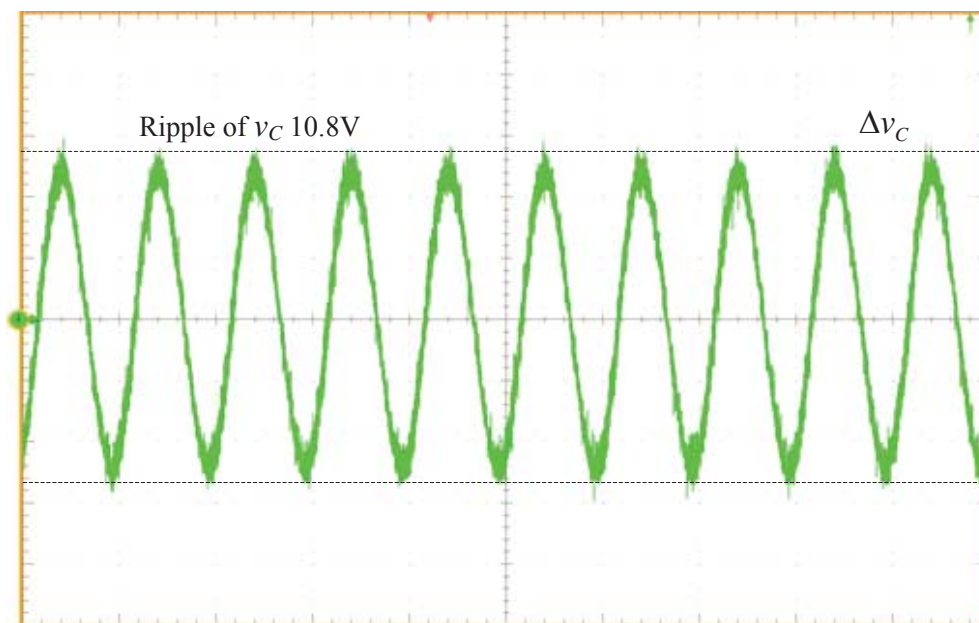
(b) Circuit schematic of the proposed module.

Fig. 9 Experimental test bed.

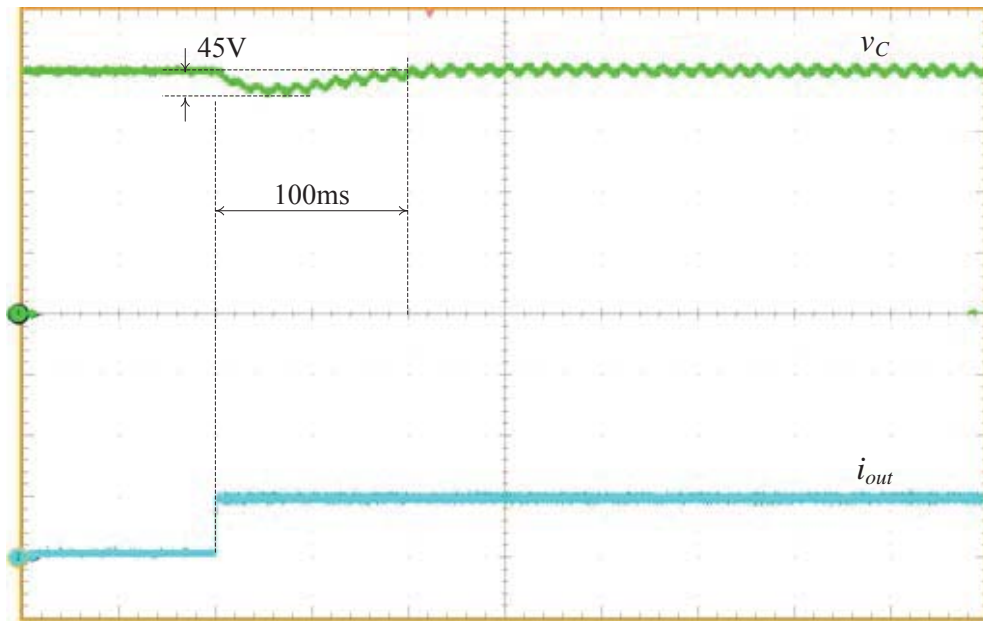




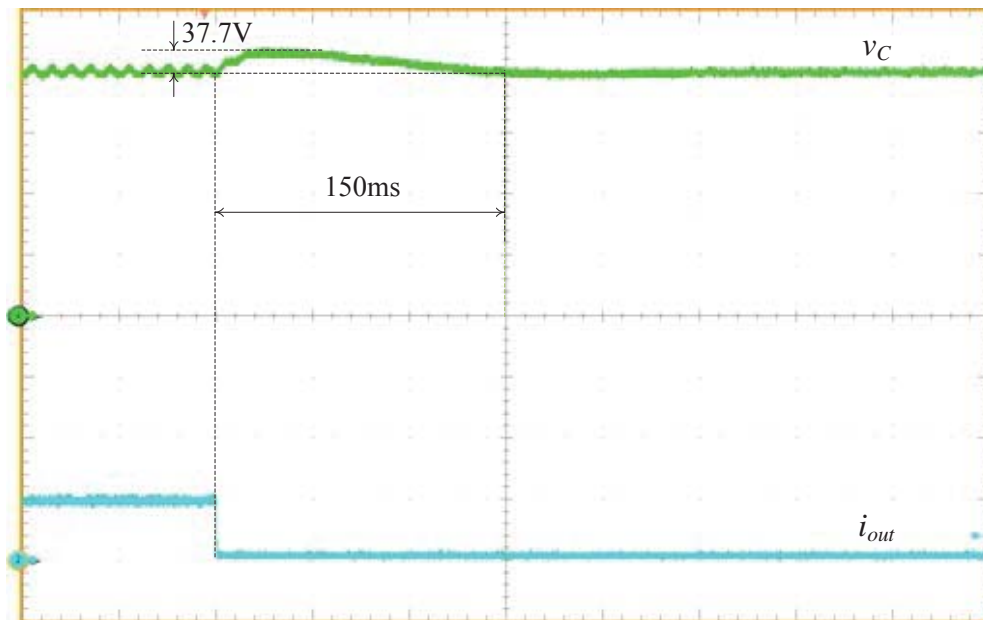
(a) Startup transient under the full load condition ( $v_C$ : 100V/div, Timebase: 50ms/div).



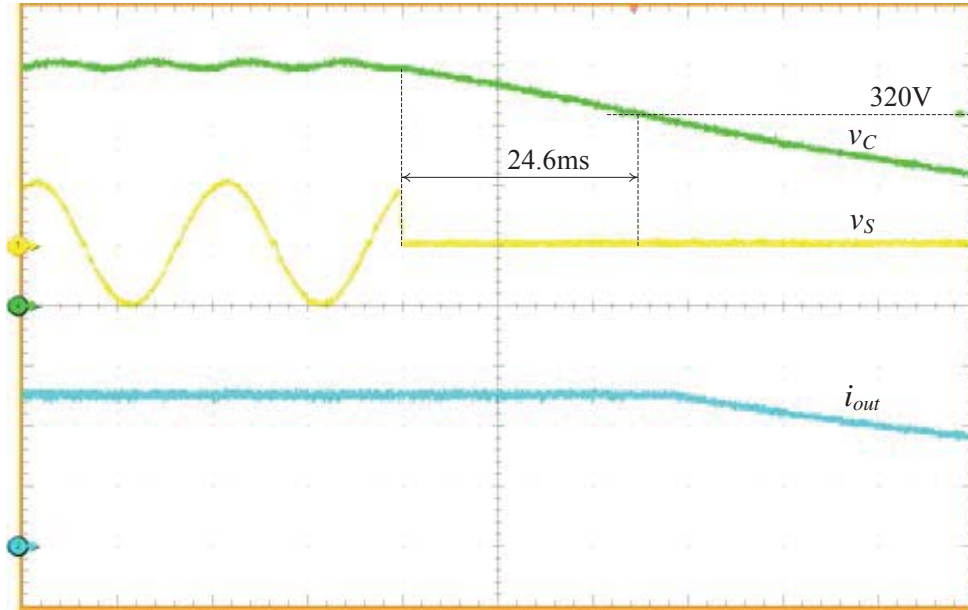
(b) Steady-state dc-link voltage waveform under the full-load condition ( $\Delta v_C$ : 2V/div, Timebase: 10ms/div).



(c) Transient waveforms when the output is changed from 10% load to full load ( $v_C$  : 100V/div,  $i_{out}$  : 50A/div, Timebase: 50ms/div).

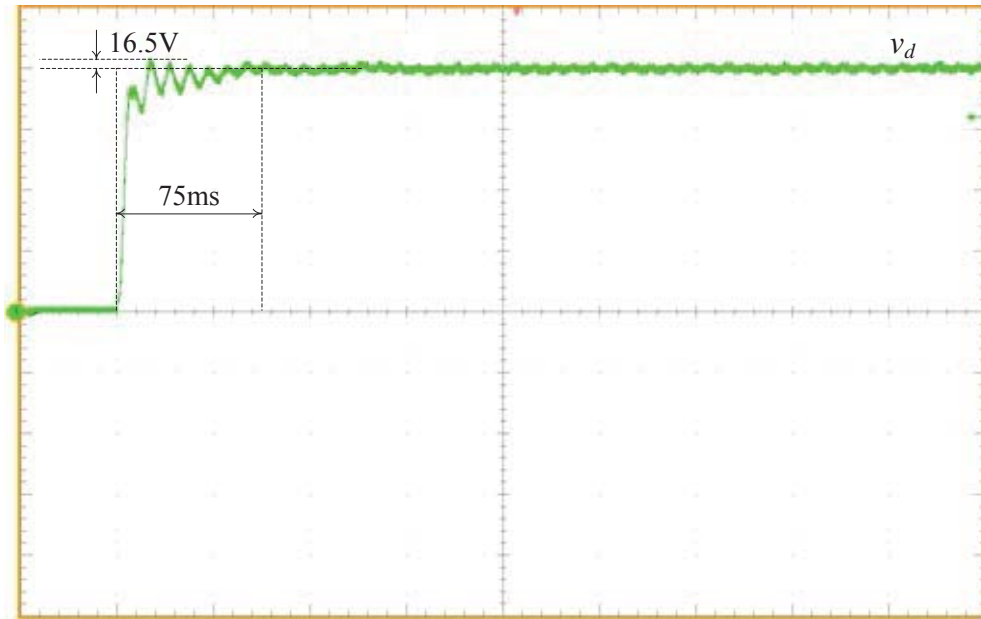


(d) Transient waveforms when the output is changed from full load to 10% load. ( $v_C$  : 100V/div,  $i_{out}$  : 50A/div, Timebase: 50ms/div).

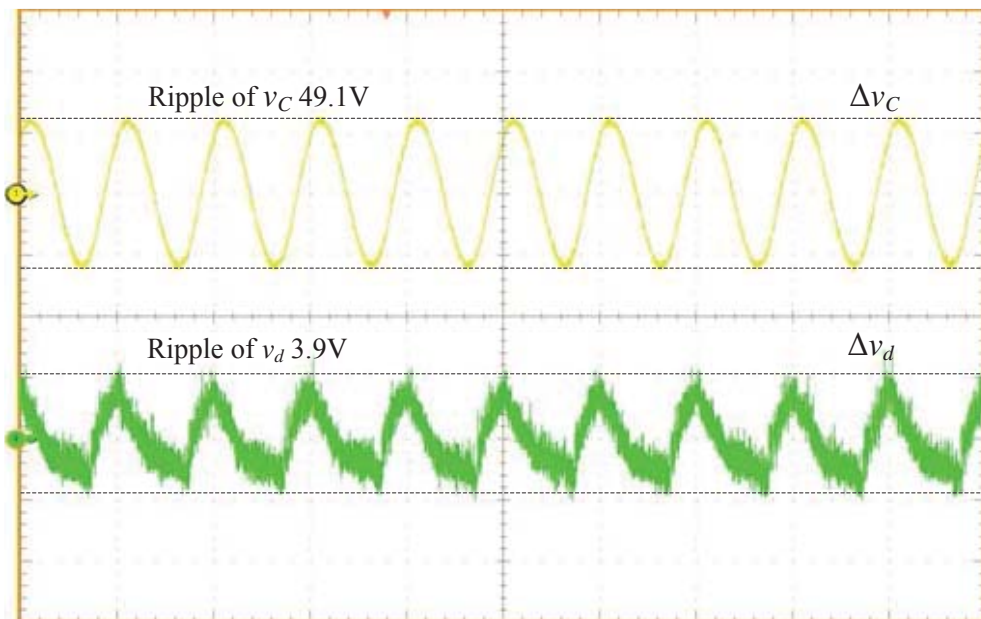


(e) Transient waveforms after a sudden supply outage under the full-load condition.  
 ( $v_C$ : 100V/div,  $v_S$ : 300V/div,  $i_{out}$ : 20A/div, Timebase: 10ms/div).

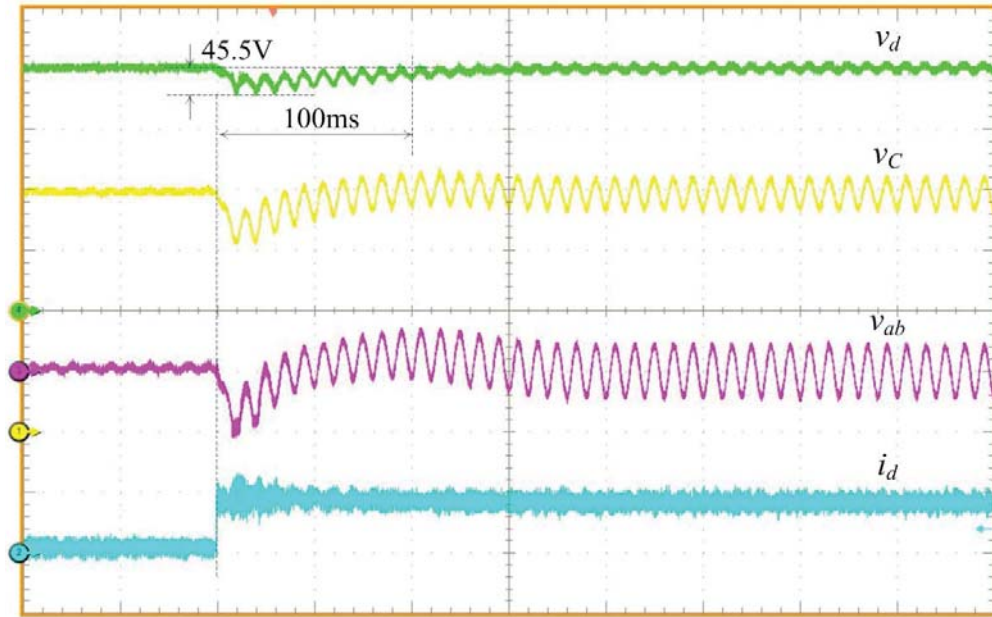
Fig. 10 Experimental waveforms with an electrolytic capacitor bank.



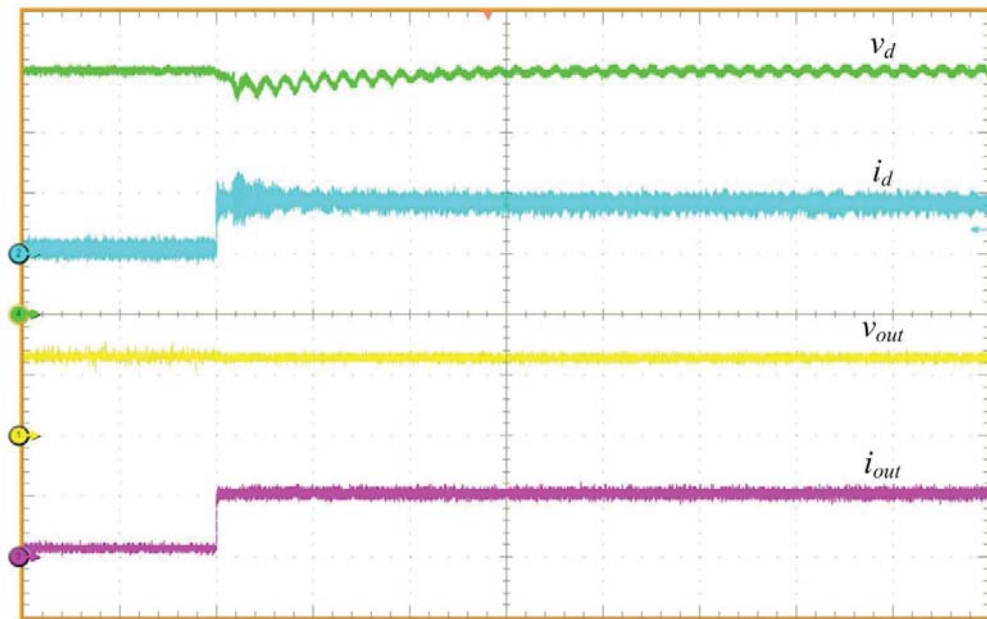
(a) Start-up transient under the full load condition. ( $v_d$ : 100V/div, Timebase: 50ms/div).



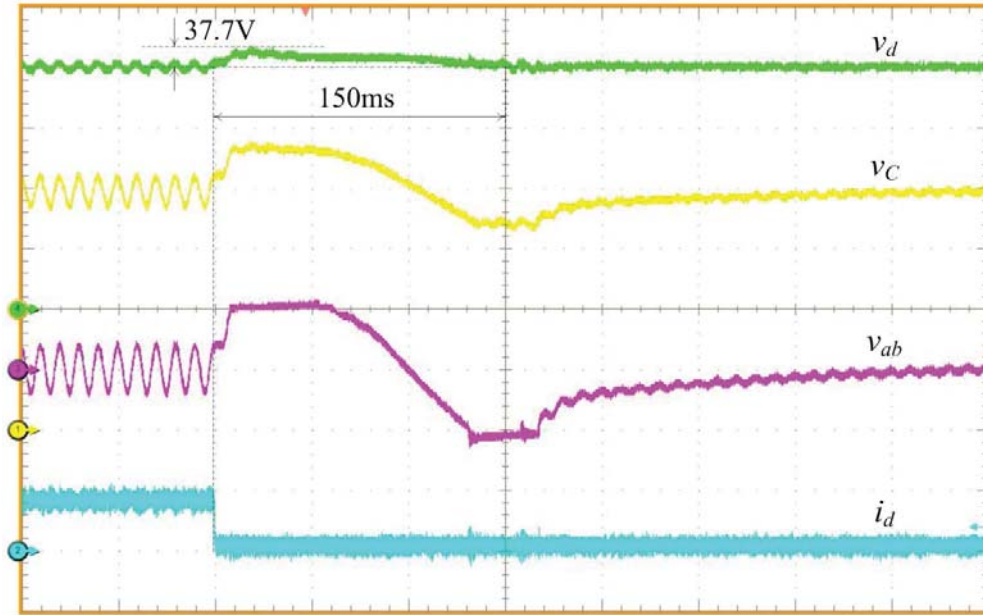
(b) Steady-state waveforms of  $v_C$  and  $v_d$  under the full-load condition  
( $\Delta v_C$ : 20V/div,  $\Delta v_d$ : 2V/div, Timebase: 10ms/div).



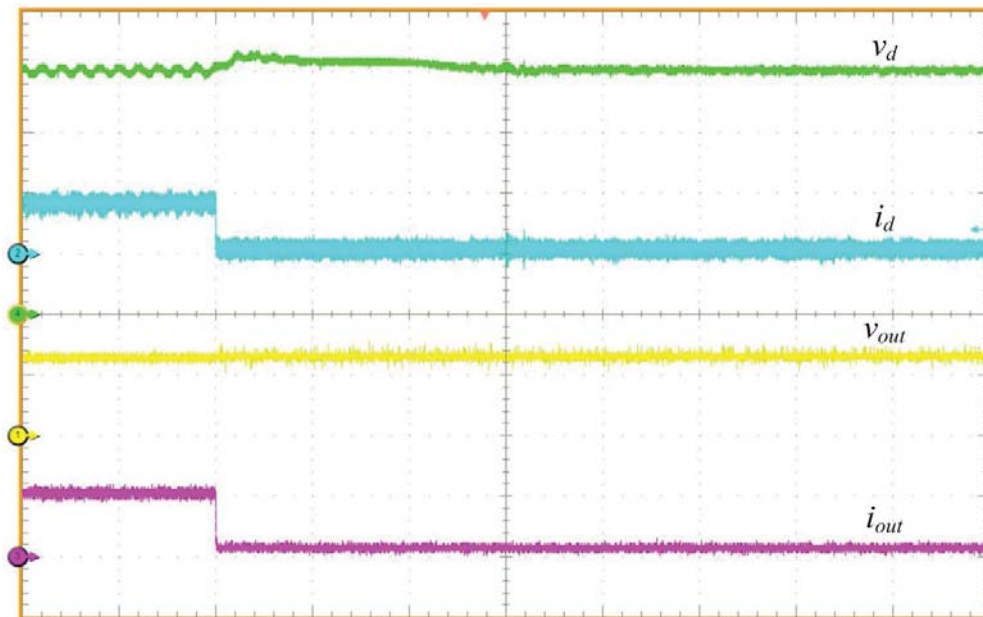
(c) Transient waveforms of the dc-link module when the output is changed from 10% load to full load ( $v_d$  : 100V/div,  $v_C$  : 100V/div,  $v_{ab}$  : 40V/div,  $i_d$  : 2A/div, Timebase: 50ms/div).



(d) Transient waveforms of the full-bridge dc-dc converter when the output is changed from 10% load to full load ( $v_d$  : 100V/div,  $i_d$  : 2A/div,  $v_{out}$  : 10V/div,  $i_{out}$  : 50A/div, Timebase: 50ms/div).

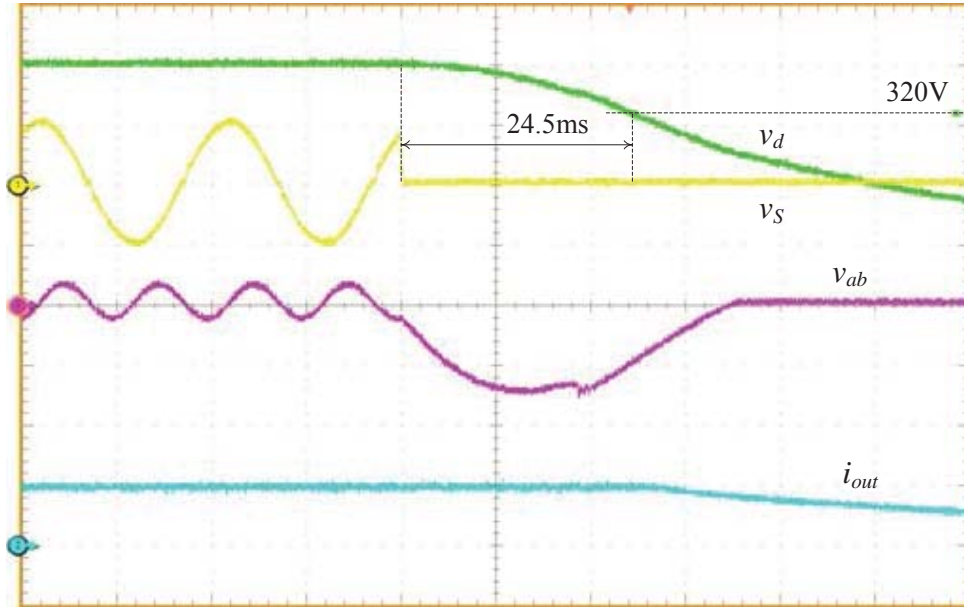


(e) Transient waveforms of the dc-link module when the output is changed from full load to 10% load ( $v_d$ : 100V/div,  $v_C$ : 100V/div,  $v_{ab}$ : 40V/div,  $i_d$ : 2A/div, Timebase: 50ms/div).



(f) Transient waveforms of the full-bridge dc-dc converter when the output is changed from full load to 10% load ( $v_d$ : 100V/div,  $i_d$ : 2A/div,  $v_{out}$ : 10V/div,  $i_{out}$ : 50A/div, Timebase: 50ms/div).





(g) Transient waveforms after a sudden supply outage under the full-load condition ( $v_d$ : 100V/div,  $v_s$ : 300V/div,  $v_{ab}$ : 20V/div,  $i_{out}$ : 50A/div, Timebase: 10ms/div).

Fig. 11 Experimental waveforms with the proposed dc-link module.

Table I – Values of the components used in the module

Parameter	Value / part no.	Parameter	Value / part no.
$C_f$	3.3 $\mu$ F, 100V	$L_f$	120 $\mu$ H
$C_a$	10 $\mu$ F, 35V	$R_a$	100k $\Omega$
$C_b$	0.1 $\mu$ F, 50V	$R_b$	33k $\Omega$
$S_1 - S_4$	FDD86102	$K$	0.1